Pyruvate kinase isoform expression alters nucleotide synthesis to impact cell proliferation

Running title: Pyruvate kinase regulates nucleotide synthesis

Sophia Y. Lunt[1,2], Vinayak Muralidhar[1,3], Aaron M. Hosios[1,4], William J. Israelsen[1,4], Dan Y. Gui[1,4], Lauren Newhouse[2], Martin Ogrodzinski[2,5], Vivian Hecht[1,6], Kali Xu[1], Paula N. Marín Acevedo[1], Daniel P. Hollern[2], Gary Bellinger[1], Talya L. Dayton[1,4], Stefan Christen[7,8], Ilaria Elia[7,8], Anh T. Dinh[1], Gregory Stephanopoulos[9], Scott R. Manalis[1,6], Michael B. Yaffe[1,4,6], Eran R. Andrechek[2], Sarah-Maria Fendt[7,8], Matthew G. Vander Heiden[1,4,10]*

1. Koch Institute for Integrative Cancer Research, Massachusetts Institute of Technology, Cambridge, MA 02139, USA.
2. Department of Physiology, Michigan State University, East Lansing, MI 48824, USA.
3. Harvard-MIT Health Sciences and Technology Division, Harvard Medical School, Boston, MA 02115, USA.
4. Department of Biology, Massachusetts Institute of Technology, Cambridge, MA 02139, USA.
5. College of Human Medicine, Michigan State University, East Lansing, MI, 48824, USA.
6. Department of Biological Engineering, Massachusetts Institute of Technology, Cambridge, MA 02139, USA.
7. Vesalius Research Center, VIB, 3000 Leuven, Belgium.
8. Department of Oncology, KU Leuven, 3000 Leuven, Belgium.
9. Department of Chemical Engineering, Massachusetts Institute of Technology, Cambridge, MA 02139, USA.
10. Dana-Farber Cancer Institute, Boston, MA 02115, USA.

* Correspondence:
Matthew G. Vander Heiden
Koch Institute for Integrative Cancer Research at Massachusetts Institute of Technology
Cambridge, MA 02139, USA
Tel: +1 617 715 4471
Fax: +1 617 253 3189
E-mail: mvh@mit.edu

SUMMARY

Metabolic regulation influences cell proliferation. The influence of pyruvate kinase isoforms on tumor cells has been extensively studied, but whether PKM2 is required for normal cell proliferation is unknown. We examine how PKM2-deletion affects proliferation and metabolism in non-transformed, non-immortalized PKM2-expressing primary cells. We find that deletion of PKM2 in primary cells results in PKM1 expression and proliferation arrest. PKM1 expression, rather than PKM2 loss, is responsible for this effect, and proliferation arrest cannot be explained by cell differentiation, senescence, death, changes in gene expression, or prevention of cell growth. Instead, PKM1 expression impairs nucleotide production and the ability to synthesize DNA and progress through the cell cycle. Nucleotide biosynthesis is limiting, as proliferation arrest is characterized by severe thymidine depletion, and supplying exogenous thymine rescues both nucleotide levels and cell proliferation. Thus, PKM1 expression promotes a metabolic state that is unable to support DNA synthesis.

INTRODUCTION

Proliferating cells metabolize glucose via aerobic glycolysis (Cairns et al., 2011; Hanahan and Weinberg, 2011; Koppenol et al., 2011). Aerobic glycolysis is characterized by increased glucose uptake and lactate excretion in the presence of oxygen, and has been proposed to promote the use of glucose for biosynthetic pathways necessary for cell growth and division (Lunt and Vander Heiden, 2011; Ward and Thompson, 2012); however, connections between aerobic glycolysis and specific pathway use are not well defined. The M2 isoform of the glycolytic enzyme pyruvate kinase (PKM2) has been associated with both aerobic glycolysis and anabolic metabolism in cancer cells (Anastasiou et al., 2012; Christofk et al., 2008a; Mazurek, 2011). PKM2 is also expressed in normal proliferating tissues (Mazurek, 2011); yet how pyruvate kinase isoform expression influences cell metabolism to support proliferation, and whether PKM2 is required for normal cell proliferation is unclear.

Pyruvate kinase converts phosphoenolpyruvate and ADP to pyruvate and ATP in glycolysis. Four isoforms of pyruvate kinase exist in mammals; each with varying kinetic and regulatory properties adapted for different tissue types. The *PKLR* gene uses two different promoters with alternative first exons to produce either the R isoform found in red blood cells, or the L isoform expressed in gluconeogenic tissues such as the liver and kidney (Domingo et al., 1992; Noguchi et al., 1987). The M1 and M2 isoforms are produced by mutually exclusive alternative mRNA splicing of the *PKM* gene. Including exon 9 in the transcript generates PKM1, while including exon 10 generates PKM2 (Noguchi et al., 1986; Yamada and Noguchi, 1999). PKM2 is found in early embryonic cells, normal proliferating cells, and tumor cells, as well as in white fat, lung, retina, and

pancreatic islets (Imamura and Tanaka, 1982; Mazurek, 2011). PKM1 replaces PKM2 during development in tissues with high ATP production requirements including skeletal muscle, heart, and brain (Imamura et al., 1986; Mazurek, 2011). When cell proliferation is reactivated in non-proliferating tissues that do not express PKM2, such as during liver regeneration or carcinogenesis, PKM2 expression is observed (Hacker et al., 1998; Steinberg et al., 1999; Van Veelen et al., 1977; Yamada and Noguchi, 1995), implying PKM2 may be important for proliferation.

PKM1 and PKM2 exhibit different regulatory and catalytic properties. PKM1 is not allosterically regulated and assembles into stable homotetramers with high pyruvate kinase activity (Gui et al., 2013; Mazurek, 2011). In contrast, PKM2 can exist in an inactive non-tetrameric form or active tetrameric form, and these states can be regulated by phosphotyrosine signaling, redox status, acetylation, and metabolic intermediates including FBP, amino acids, SAICAR, and fatty acids (Anastasiou et al., 2011; Anastasiou et al., 2012; Chaneton et al., 2012; Christofk et al., 2008b; Keller et al., 2012; Lv et al., 2011). In addition, several non-glycolytic functions specific for PKM2 have been reported to be critical for cancer cell proliferation (Gao et al., 2012; Jiang et al., 2014; Keller et al., 2014; Luo et al., 2011; Yang et al., 2012a; Yang et al., 2011; Yang et al., 2012b), but it is unclear if any of these functions are important for proliferation of normal cells.

Here, we use non-immortalized primary cells from PKM2-conditional mice to study the role of PKM1 and PKM2 isoform expression in cell metabolism and proliferation. Deletion of PKM2 in these cells results in PKM1 expression and proliferation arrest. Expression of PKM1 in cells that co-express PKM2 also results in

proliferation arrest, suggesting that expression of PKM1, rather than loss of PKM2, is responsible for this phenotype. Proliferation arrest is not associated with cell differentiation, senescence, changes in gene expression, or death; instead, PKM1 expression results in decreased flux to select biosynthetic pathways with nucleotide synthesis being a critical pathway that is limiting for cell proliferation. Proliferation arrest can be rescued by exogenous pyrimidine or purine base supplementation. These data argue that PKM1 expression suppresses nucleotide biosynthesis, and that PKM2 expression supports flux into metabolic pathways to support DNA synthesis.

RESULTS

PKM1 expression causes proliferation arrest of primary embryonic fibroblasts

To study the role of PKM2 in cell proliferation, we derived embryonic fibroblasts (MEFs) from mice where LoxP sites flank PKM2-specific exon 10 (*PKM2*$^{fl/fl}$) and harbor an inducible Cre recombinase allele (*Cre-ER*) (Israelsen et al., 2013). Deletion of exon 10 disrupts the ability of cells to produce PKM2 or any truncated protein product with PKM2 activity, but does not prevent production of PKM1 (Israelsen et al., 2013). When Cre recombinase remains inactive, PKM2 is expressed in *PKM2*$^{fl/fl}$ *Cre-ER* cells (Figure 1A), as reported for wildtype MEFs (Anastasiou et al., 2011). Addition of 4-hydroxytamoxifen (4-OHT) activates Cre recombinase, leading to loss of PKM2 protein and PKM1 expression (Figure 1A). PKM1 expression is observed one day after 4-OHT treatment; however, residual PKM2 can be detected for up to 4 days following 4-OHT

treatment, presumably due to the half-life of PK protein being as long as 104 hours (Illg and Pette, 1979; Yee et al., 2010).

Similar to wildtype MEFs, primary *PKM2*$^{fl/fl}$ *Cre-ER* MEFs proliferate rapidly in culture for multiple passages (Figure 1B). When treated with 4-OHT, these MEFs exhibit a marked decrease in proliferation (Figure 1B). A similar proliferation arrest was observed in multiple lines, each independently derived from different *PKM2*$^{fl/fl}$ *Cre-ER* mice (Figure S1A). To ensure that 4-OHT treatment itself is not affecting PK isoform expression or cell proliferation, we generated MEFs from *PKM2*$^{fl/fl}$ mice that do not harbor a *Cre-ER* allele. These Cre-negative *PKM2*$^{fl/fl}$ MEFs express PKM2 (Figure S1B) and proliferate at a similar rate regardless of 4-OHT treatment (Figure 1C).

To determine whether expression of PKM1 or loss of PKM2 is responsible for cell proliferation arrest, we derived MEFs from *PKM2*$^{fl/+}$ *Cre-ER* mice. Without 4-OHT treatment, these MEFs express only PKM2 (Figure 1D) and proliferate for several passages (Figure 1E). 4-OHT treatment of *PKM2*$^{fl/+}$ *Cre-ER* MEFs causes deletion of the PKM2 conditional allele and results in expression of PKM1 with continued PKM2 expression from the wildtype allele (Figure 1D). As observed in *PKM2*$^{fl/fl}$ *Cre-ER* MEFs, 4-OHT addition caused a similar proliferation arrest in *PKM2*$^{fl/+}$ *Cre-ER* MEFs despite retention of PKM2 expression (Figure 1E). Cre expression alone can also slow proliferation without affecting pyruvate kinase isoform expression, but does not increase γ-H2AX levels and has less impact on cell proliferation than Cre-mediated PKM2 deletion (Figure S1C-S1E). To test whether the increase in pyruvate kinase activity associated with gain of PKM1 expression contributes to a block in proliferation, we monitored proliferation of wildtype MEFs following addition of the small molecule PKM2

activator TEPP-46 (Anastasiou et al., 2012). TEPP-46 decreases proliferation (Figure 1F), and exogenous PKM1 cDNA expression also reduces proliferation of wildtype MEFs (Figure S1F). Together, these data suggest proliferation is suppressed in *PKM2*$^{\Delta/\Delta}$ MEFs due to gain of PKM1 rather than loss of PKM2.

Deletion of PKM2 does not induce cell death, senescence, or differentiation

Potential explanations for why PKM1 expression suppresses proliferation include an increase in cell death, cell senescence, and/or differentiation to a non-proliferating cell population. To begin to examine these possibilities in cells with and without PKM2 deletion, we quantified the percentage of viable cells by propidium iodide exclusion and the amount of cell death by lactate dehydrogenase release (Decker and Lohmann-Matthes, 1988; Nicoletti et al., 1991). No difference in cell viability or LDH release was found between *PKM2*$^{fl/fl}$ and *PKM2*$^{\Delta/\Delta}$ MEFs as late as 9 days after vehicle or 4-OHT treatment despite a large difference in cell number (Figures 2A and S2A). Consistent with these results, >90% of MEFs from both populations exclude trypan blue at this time point. These data suggest PKM1 expression following PKM2-deletion inhibits cell proliferation without increasing cell death.

Primary MEFs undergo senescence upon serial passage in culture that involves entry into a state of irreversible proliferation arrest (Campisi, 2011; Kuilman et al., 2010; Odell et al., 2010). Therefore, it was possible that PKM1 expression induces early senescence. One marker of senescent cells is acid-stable β-galactosidase activity (Castro et al., 2003; Dimri et al., 1995; van der Loo et al., 1998). No difference in acid-stable β-galactosidase activity was found between early passage proliferating *PKM2*$^{fl/fl}$

and proliferation-arrested *PKM2*$^{\Delta/\Delta}$ MEFs as late as 9 days after treatment with vehicle or 4-OHT (Figure 2B, upper panels). Late passage *PKM2*$^{fl/fl}$ MEFs senesce as evidenced by proliferation arrest, morphology change, and acid-stable β-galactosidase staining. Surprisingly, despite no proliferation for days, *PKM2*$^{\Delta/\Delta}$ MEFs stain positive for acid-stable β-galactosidase activity at the same time *PKM2*$^{fl/fl}$ MEFs senesce due to high passage number (Figure 2B, lower panels). These data suggest induction of the senescence program observed with serial primary cell passage does not correlate with proliferation arrest of *PKM2*$^{\Delta/\Delta}$ cells.

Primary MEFs can differentiate under specific culture conditions. For instance, MEFs can differentiate along an adipocyte-like lineage and accumulate neutral lipids (Green and Kehinde, 1974; Russell and Ho, 1976). To determine if *PKM2*$^{\Delta/\Delta}$ MEFs accumulate lipids, we stained them with Oil Red O and found no evidence of lipid accumulation (Figure S2B). To further test whether *PKM2* deletion causes differentiation, and determine whether proliferation arrest is observed in *PKM2*$^{\Delta/\Delta}$ primary cells other than MEFs, we isolated myoblasts from *PKM2*$^{fl/fl}$ *Cre-ER* mice. Myoblasts can be induced to differentiate into myotubes with characteristic morphology (Wakelam, 1985), and are a well-studied differentiation model (Abmayr and Pavlath, 2012). Similar to the phenotype observed in *PKM2*$^{fl/fl}$ *Cre-ER* MEFs, treatment of *PKM2*$^{fl/fl}$ *Cre-ER* myoblasts with 4-OHT results in PKM2 deletion and PKM1 expression (Figure S2C) with proliferation arrest (Figure 2C). Similar to immortalized C2C12 myoblasts (Clower et al., 2010), we confirmed primary *PKM2*$^{fl/fl}$ *Cre-ER* myoblasts are capable of differentiation under conditions that favor myotube formation (Figure 2D) and

express PKM1 upon differentiation (Figure S2D). However, PKM2 deletion in myoblasts does not cause differentiation into myotubes (Figure 2D).

PKM2$^{\Delta/\Delta}$ MEFs do not incorporate EdU

Lack of *PKM2*$^{\Delta/\Delta}$ MEF proliferation implies an inability to proceed through the cell cycle. To investigate whether *PKM2*$^{\Delta/\Delta}$ MEFs replicate DNA, they were incubated with EdU, a thymidine analog incorporated into DNA during S phase of the cell cycle. Consistent with lack of DNA synthesis, *PKM2*$^{\Delta/\Delta}$ MEFs exhibit decreased EdU incorporation compared to *PKM2*$^{fl/fl}$ MEFs (Figure 2E). Cells deprived of nutrients classically arrest in G1 phase of the cell cycle (Bohnsack and Hirschi, 2004). To determine whether *PKM2*$^{\Delta/\Delta}$ MEFs were arrested in G1, we analyzed DNA content by flow cytometry. Both the G1 and G2/M phase DNA content peaks widened in a pattern that is most consistent with more cells in S phase (Figure 2F). Dual staining of EdU incorporation and DNA content is also consistent with an inability to progress through the cell cycle, as less EdU incorporation is observed at all DNA contents, with much of the population having a DNA content between 2N and 4N despite no EdU uptake (Figure 2G). To compare *PKM2*$^{\Delta/\Delta}$ MEF arrest to cell cycle arrest induced by nutrient withdrawal, the DNA content of wildtype MEFs was assessed following removal of the essential amino acid lysine. Lysine withdrawal also causes proliferation arrest (Figure S2E); however, unlike *PKM2*$^{\Delta/\Delta}$ MEFs, these cells accumulate in G1 (Figures S2F). Taken together, these results argue that lack of proliferation caused by PKM1 expression is distinct from G1 arrest caused by nutrient deprivation. Instead, these data

are more consistent with a failure of *PKM2*$^{\Delta/\Delta}$ MEFs to incorporate nucleotides into DNA.

Despite proliferation arrest, *PKM2*$^{\Delta/\Delta}$ MEFs continue to uptake nutrients and grow

Cell division can depend on cell size in eukaryotic cells (Johnston et al., 1977; Montagne et al., 1999). A possible explanation for why cells stop proliferating is that changes in metabolism lead to insufficient metabolic precursors to support cell growth, and sufficient size to complete a cell cycle is not achieved. To determine whether proliferation arrest of *PKM2*$^{\Delta/\Delta}$ MEFs is associated with decreased aerobic glycolysis, we measured consumption of glucose as well as lactate excretion. Surprisingly, despite proliferation arrest, *PKM2*$^{\Delta/\Delta}$ MEFs have higher glucose uptake and lactate excretion rates than *PKM2*$^{fl/fl}$ MEFs (Figures 3A and 3B). Overall glucose oxidation is also increased in *PKM2*$^{\Delta/\Delta}$ MEFs: measurement of $^{14}CO_2$ production from uniformly radiolabeled glucose revealed ~40% more $^{14}CO_2$ production from glucose over 24-hours in *PKM2*$^{\Delta/\Delta}$ MEFs than in *PKM2*$^{fl/fl}$ MEFs (Figure 3C). In addition, assessment of cell volume showed that *PKM2*$^{\Delta/\Delta}$ cells are ~1.7 times larger than proliferating *PKM2*$^{fl/fl}$ cells (Figure 3D). In fact, the mean volume of arrested *PKM2*$^{\Delta/\Delta}$ cells was larger than 85% of cycling *PKM2*$^{fl/fl}$ cells, suggesting *PKM2*$^{\Delta/\Delta}$ MEFs grow to a large size despite proliferation arrest. The cell volume increase is accompanied by increased protein amount, with total protein content of *PKM2*$^{\Delta/\Delta}$ MEFs ~1.9 times greater than total protein content in cycling *PKM2*$^{fl/fl}$ MEFs (Figure 3E). *PKM2*$^{\Delta/\Delta}$ MEFs also contain higher levels of fatty acids, with pool sizes of palmitate, oleate, and sterate > 2-fold higher in *PKM2*$^{\Delta/\Delta}$ MEFs compared to *PKM2*$^{fl/fl}$ MEFs (Figure S3). To confirm that increases in cell volume,

total protein, and select fatty acids are accompanied by an increase in cell mass, we utilized a suspended microchannel resonator (Burg et al., 2007) to determine dry mass at the single cell level (Feijo Delgado et al., 2013). The dry mass of *PKM2*$^{\Delta/\Delta}$ cells is greater than the dry mass of *PKM2*$^{fl/fl}$ cells (783 pg for *PKM2*$^{\Delta/\Delta}$ MEFs compared to 455 pg for *PKM2*$^{fl/fl}$ MEFs; Figure 3F). One million *PKM2*$^{\Delta/\Delta}$ MEFs also weighed 24 ± 4% more than the same number of *PKM2*$^{fl/fl}$ MEFs when dried on filter paper and weighed using an analytical balance. Together, these data suggest that despite proliferation arrest, *PKM2*$^{\Delta/\Delta}$ MEFs continue to metabolize glucose at high rates and grow to a larger size than proliferating *PKM2*$^{fl/fl}$ MEFs.

PKM2 supports specific aspects of anabolic metabolism

Despite growing to a larger size, specific metabolite(s) or metabolic flux limitations could account for the inability of *PKM2*$^{\Delta/\Delta}$ cells to proliferate. To explore this hypothesis, we used isotope labeled nutrients and mass spectrometry-based metabolite analysis to probe metabolism of *PKM2*$^{\Delta/\Delta}$ MEFs in comparison to *PKM2*$^{fl/fl}$ MEFs. Analysis of intracellular metabolites after culture in the presence of uniformly labeled ^{13}C-glucose ([U-$^{13}C_6$]glucose) and glutamine ([U-$^{13}C_5$]glutamine) reveals that *PKM2*$^{\Delta/\Delta}$ MEFs have decreased labeling from glucose and glutamine in some biosynthetic precursors including the nucleotide uridine monophosphate (UMP) and the fatty acid palmitate (Figures 4 and S4). Moreover, ^{13}C-glucose incorporation into serine and glycine were also decreased in *PKM2*$^{\Delta/\Delta}$ MEFs. In contrast, a higher percentage of TCA cycle intermediates are labeled from [U-$^{13}C_6$]glucose in *PKM2*$^{\Delta/\Delta}$ MEFs (Figure 4A), suggesting increased glucose contribution and/or decreased glutamine contribution to

the TCA cycle. Labeling studies using [U-$^{13}C_5$]glutamine show that *PKM2*$^{\Delta/\Delta}$ MEFs have lower glutamine contribution to TCA cycle intermediates (Figure 4B), implying that proliferation-arrested *PKM2*$^{\Delta/\Delta}$ MEFs rely more on glucose than glutamine to support the TCA cycle. These results confirm that PKM1 expression leads to increased glucose catabolism, and support a model where PKM1 expression curtails the use of glucose and glutamine for production of some biosynthetic precursors.

Glucose is the major precursor for *de novo* palmitate synthesis in both *PKM2*$^{\Delta/\Delta}$ and *PKM2*$^{fl/fl}$ MEFs, despite less palmitate synthesized from both glucose and glutamine in *PKM2*$^{\Delta/\Delta}$ MEFs relative to *PKM2*$^{fl/fl}$ MEFs (Figure S4). The rate of total fatty acid synthesis decreased by 22% with PKM2 deletion in these cells, consistent with decreased lipid synthesis observed previously upon PKM1 expression (Anastasiou et al., 2012). A fraction of palmitate is produced from glutamine in *PKM2*$^{fl/fl}$ and *PKM2*$^{\Delta/\Delta}$ MEFs, with a labeling pattern consistent with synthesis by reductive metabolism in both cases (Fendt et al., 2013b; Metallo et al., 2012). Although *PKM2*$^{\Delta/\Delta}$ MEFs exhibit decreased fatty acid synthesis, they contain higher levels of intracellular fatty acids compared to their *PKM2*$^{fl/fl}$ counterparts (Figure S3). To accumulate high levels of fatty acids despite a decrease in biosynthesis, it is likely that *PKM2*$^{\Delta/\Delta}$ MEFs import exogenous fatty acids. Lipid scavenging from the media has been observed previously in cancer cells (Kamphorst et al., 2013).

Proliferation of *PKM2*$^{\Delta/\Delta}$ MEFs is limited by nucleotides

Pool sizes of intracellular metabolites were measured to assess whether specific metabolites are limiting for cell proliferation in *PKM2*$^{\Delta/\Delta}$ MEFs. While levels of most

metabolites in *PKM2*$^{\Delta/\Delta}$ cells were unchanged or increased relative to *PKM2*$^{fl/fl}$ cells (Figure S5A), nucleotide levels were lower, and the most depleted intracellular metabolite measured in *PKM2*$^{\Delta/\Delta}$ MEFs is thymidine monophosphate (dTMP; Figure 5A). This is consistent with decreased glucose and glutamine contribution to UMP observed in *PKM2*$^{\Delta/\Delta}$ MEFs (Figure 4), as UMP is a biosynthetic precursor of dTMP.

To explore the possibility that *de novo* nucleotide synthesis is decreased in *PKM2*$^{\Delta/\Delta}$ MEFs, we performed dynamic labeling experiments and flux modeling. Dynamic labeling with uniformly labeled ^{13}C-glucose and ^{13}C-glutamine confirms decreased glucose and glutamine flux to UMP in *PKM2*$^{\Delta/\Delta}$ MEFs (Figure 5B). The same labeling studies also suggest flux of glucose carbon into IMP and AMP is decreased slightly in *PKM2*$^{\Delta/\Delta}$ MEFs, while glutamine labeling is not informative as this amino acid does not contribute carbons to *de novo* purine synthesis. Analysis of metabolic fluxes from steady state labeling data (Antoniewicz et al., 2007; Young et al., 2008) support the notion that *de novo* nucleotide synthesis, glutamine to glutamate conversion, and 3-phosphoglycerate (3PG) to serine flux are decreased in *PKM2*$^{\Delta/\Delta}$ MEFs (Figure 5C). Decreased 3PG to serine flux is consistent with previous reports of PKM2 expression shunting carbon into serine biosynthesis (Chaneton et al., 2012); however, despite decreased serine synthesis, serine levels remained unchanged (Figure S5A). To determine if serine metabolism could be limiting for *de novo* nucleotide biosynthesis, we modeled fluxes for serine-glycine-one carbon metabolism based on ^{13}C-glucose incorporation into serine and glycine as well as serine and glycine uptake rates from the media (Figure S5B, Supplementary Material). While decreased 3PG conversion to serine was suggested by the model in *PKM2*$^{\Delta/\Delta}$ MEFs, serine uptake appeared sufficient

to compensate for any decrease in *de novo* serine synthesis, suggesting that a lack of serine availability alone is unlikely to account for impaired nucleotide synthesis.

Proliferation arrest of *PKM2*$^{\Delta/\Delta}$ MEFs is not caused by gene expression changes

We performed genome-scale gene expression analysis to explore whether changes in gene expression cause *PKM2*$^{\Delta/\Delta}$ MEFs proliferation arrest. Analysis of microarray data for *PKM2*$^{\Delta/\Delta}$ and *PKM2*$^{fl/fl}$ cells obtained from two different independently derived MEF lines revealed no correlation between gene expression changes and pyruvate kinase isoform expression (Figure 6A). In fact, unsupervised hierarchical clustering results in clustering by the embryo from which the MEFs were generated rather than by pyruvate kinase isoform expression. As an additional approach, we used fold change analysis to compare gene expression differences between *PKM2*$^{\Delta/\Delta}$ and *PKM2*$^{fl/fl}$ MEFs. This analysis revealed a small number of genes that show differences according to pyruvate kinase isoform expression, and these results were confirmed by RT-PCR (Figure S6A); however, none of the genes are directly related to metabolism or cell cycle control.

Since metabolic analysis of *PKM2*$^{\Delta/\Delta}$ and *PKM2*$^{fl/fl}$ MEFs revealed deficiencies in nucleotide metabolism, we re-analyzed the gene expression data examining only nucleotide metabolism genes (Figure 6B). Again, unsupervised hierarchical clustering does not show a correlation between expression changes and pyruvate kinase isoform expression, and most genes show minimal change in expression levels. To confirm these results, we examined relative protein and gene expression levels of several key nucleotide metabolism genes by Western blotting and RT-PCR (Figures S6B and S6C).

None showed differences in expression between *PKM2*$^{\Delta/\Delta}$ and *PKM2*$^{fl/fl}$ MEFs. These results argue that changes in gene expression do not account for either impaired nucleotide synthesis or proliferation arrest of *PKM2*$^{\Delta/\Delta}$ MEFs.

PKM2$^{\Delta/\Delta}$ MEFs cannot complete DNA synthesis

To determine whether *de novo* pyrimidine production is limiting for proliferation of *PKM2*$^{\Delta/\Delta}$ MEFs, we attempted to prevent proliferation arrest by supplementing the media with thymine at the time of 4-OHT addition. Thymine supplementation prevented proliferation arrest of *PKM2*$^{\Delta/\Delta}$ MEFs (Figure 7A). Thymine supplementation also prevents depletion of intracellular dTMP and dTTP levels, as well as levels of other nucleotides (Figure 5A) and some other depleted metabolites (Figure S5A), but has no effect on proliferation of *PKM2*$^{fl/fl}$ MEFs or Cre expressing MEFs (Figures S7A and S1C). The ability of thymine supplementation to sustain proliferation of *PKM2*$^{\Delta/\Delta}$ MEFs is maintained for up to 10 days, and does not increase *PKM2*$^{\Delta/\Delta}$ MEF cell number by inducing a burst of proliferation following addition of thymine. The pyrimidines cytosine and uracil and purines inosine, guanine, and adenine also partially prevent proliferation arrest of *PKM2*$^{\Delta/\Delta}$ MEFs, but to a lesser extent (Figure 7A). To confirm that changes in serine are not limiting for cell proliferation, we supplemented *PKM2*$^{\Delta/\Delta}$ MEFs with serine; however, neither serine nor other substrates used in nucleotide synthesis rescued proliferation (Figure 7A).

To determine whether thymine supplementation can restore proliferation of arrested *PKM2*$^{\Delta/\Delta}$ MEFs, we added thymine to the media 5 days after 4-OHT addition, a

time point when PKM2-deleted cells have stopped proliferating (Figure 1B). Thymine addition restores proliferation that is sustained for several days; however, the cells senesce around day 10 and thus undergo fewer population doublings (Figure S7B). Even when media is changed every 3 days without replating, no spontaneous recovery has been observed in *PKM2*$^{\Delta/\Delta}$ MEFs despite following cultures for up to 18 days after proliferation arrest.

To determine whether DNA synthesis might be limited by nucleotide pools in *PKM2*$^{\Delta/\Delta}$ MEFs, we performed DNA labeling studies to directly visualize nucleotide incorporation into DNA over time (Figure 7B). While *PKM2*$^{fl/fl}$ MEFs incorporate both 5-Chloro-2′-deoxyuridine (CldU) and 5-Iodo-2′-deoxyuridine (IdU) to produce long DNA strands over a 20 minute period, *PKM2*$^{\Delta/\Delta}$ MEFs are only able to incorporate CldU and IdU for short bursts, and strands with both CldU and IdU are rarely observed (Figures 7B and 7C). These data suggest at least some *PKM2*$^{\Delta/\Delta}$ MEFs are in S phase because limited CldU and IdU incorporation into DNA is observed. The data also argue that *PKM2*$^{\Delta/\Delta}$ MEFs are unable to sustain DNA synthesis, and are consistent with nucleotide depletion causing proliferation arrest. Together, our experiments argue PKM1 expression leads to low nucleotide levels and an inability to replicate DNA.

DISCUSSION

While most proliferating cells express PKM2, the exact role of PKM2 in cell proliferation remains controversial. Unlike constitutively active PKM1, PKM2 can be regulated to assume either a low or high activity state, and the inactive state of PKM2 is favored in proliferating tumor cells (Israelsen et al., 2013). It has been proposed that

less active PKM2 allows buildup of upstream glycolytic metabolites that can feed into biosynthetic pathways, with the subsequent ability to use these metabolites for anabolic metabolism (Christofk et al., 2008b; Eigenbrodt and Glossmann, 1980). Consistent with this idea, our data show that expression of constitutively active PKM1 results in decreased *de novo* nucleotide biosynthesis. However, contrary to this hypothesis, PKM1 expression did not deplete upstream glycolytic intermediates or impair all anabolic metabolism. Instead, pools of upstream glycolytic intermediates and most intracellular metabolites were unchanged, and the cells continued to accumulate protein and lipids to grow to a larger size. This suggests protein and nucleotide synthesis can be uncoupled in these cells. This is in contrast to findings in some cancer cells where coordinate regulation of protein synthesis and nucleotide synthesis is observed (Cunningham et al., 2014)

PKM1 expression led to severe thymidine depletion and proliferation arrest that is rescued by thymine supplementation. Although all nucleotides were depleted, depletion of pyrimidines may be most severe because they depend on both glucose and glutamine as carbon sources, while purines only depend on glucose. Thymine supplementation was most effective; however, supplementation of other nucleotide bases could also partially prevent proliferation arrest. Nucleotide levels in cells are tightly regulated with complex allosteric control of synthesis maintaining balanced pools in cells such that changes in one nucleotide pool can impact the availability of other nucleotides (Cohen et al., 1983; Reichard, 1988). Although pyrimidines and purines cannot be interconverted, changes in pyrimidine production impacts both purine and pyrimidine levels (Reaves et al., 2013). Methotrexate impairs thymidine synthesis and

depletes both purines and pyrimidines in tumor cells (Hryniuk, 1975; Hryniuk et al., 1975; Tattersall et al., 1974). Thymidine supplementation alone rescues methotrexate toxicity in some cancer cells, while others require both purine and pyrimidine supplementation (Harrap et al., 1977).

Thymidine depletion is the basis for anti-proliferative therapies that range from antibiotics (Hawser et al., 2006; Kwon et al., 2010) to cancer chemotherapy (Gangjee et al., 2007; Witherspoon et al., 2013). The success of drugs that target thymidine pools highlights the importance of generating this nucleotide in proliferating cells. Nucleotide depletion can trigger cell cycle arrest in human neuroblastoma cell lines (Messina et al., 2004) and T lymphocytes (Laliberté et al., 1998). Similar to our findings, proliferation arrest induced by nucleotide depletion in T lymphocytes could be reversed with nucleotide supplementation (Turka et al., 1991). Accumulation of cells in S phase and a slow DNA replication rate has also been observed in cells treated with hydroxyurea, a ribonucleotide reductase inhibitor that lowers deoxynucleotide pools (Anglana et al., 2003). Additional studies have shown low nucleotides can impair cancer progression (Cunningham et al., 2014) or cause oncogene-induced senescence (Aird et al., 2013), suggesting nucleotide levels can limit proliferation in other contexts.

Some mammalian cells can continue DNA synthesis with imbalanced deoxyribonucleoside pools (Meuth, 1989); however, nucleotide insufficiency can also result in DNA polymerase stalling, collapsed replication forks, and activation of the DNA damage response (Bester et al., 2011). Activation of the DNA damage response is one mechanism that could account for S-phase cell cycle arrest in *PKM2*$^{\Delta/\Delta}$ cells, although increased γ-H2AX staining was not observed. The lack of sustained DNA replication in

PKM2$^{\Delta/\Delta}$ cells suggests they enter S-phase with insufficient nucleotides to complete this phase of the cell cycle. It has been suggested that one function of the G1-S cell size check point is to ensure sufficient nutrients are available to complete S-phase (Foster et al., 2010), while others have argued that mammalian cells only have sufficient precursor stores to sustain DNA replication for a few minutes and therefore must continuously replenish deoxynucleotide pools to replicate the genome (Reichard, 1988). These data argue that regulation of pyruvate kinase isoform expression can impact the ability of cells to generate nucleotides and progress through S-phase.

To avoid a high mutation rate, cells may decrease oxidative metabolism during S-phase to protect the genome from DNA damage (Tu et al., 2005). PKM2 expression can favor the use of aerobic glycolysis (Christofk et al., 2008a); however, apart from protecting the genome by limiting oxidative phosphorylation, these data imply that aerobic glycolysis may also be important for supporting nucleotide synthesis to complete S-phase. Supporting nucleotide production may be another mechanism by which aerobic glycolysis keeps the mutation rate low by preventing collapsed replication forks caused by insufficient nucleotides.

Serine activates PKM2 and decreases new serine synthesis (Chaneton et al., 2012). Increased pyruvate kinase activity from PKM1 expression decreases 3PG to serine flux; however, serine levels are not affected in these cells despite decreased serine production. In fact, serine levels are maintained despite increased protein and cell mass in *PKM2*$^{\Delta/\Delta}$ relative to *PKM2*$^{fl/fl}$ MEFs.

Non-metabolic functions of PKM2 have also been reported (Gao et al., 2012; Keller et al., 2014; Luo et al., 2011; Yang et al., 2012a; Yang et al., 2011; Yang et al.,

2012b), including a role for PKM2 in regulating mitosis (Jiang et al., 2014). However, the failure of most *PKM2*$^{\Delta/\Delta}$ MEFs to arrest in G2/M, and the ability to rescue proliferation with thymine supplementation both argue defects in chromosome segregation are not a major cause of proliferation arrest in these cells. Because most non-metabolic PKM2 functions are proposed to alter gene expression, the observation that loss of PKM2 causes minimal gene expression changes suggests that these PKM2 activities are less active in primary MEFs.

The inability of *PKM2*$^{\Delta/\Delta}$ MEFs to sustain DNA synthesis is consistent with a model where a switch from PKM2 to PKM1 expression leads to low deoxynucleotide levels, an inability to replicate DNA, and decreased proliferation without affecting cell mass accumulation. How pyruvate kinase activity regulates nucleotide biosynthesis remains unknown. PKM2 can influence ribose production via the oxidative pentose phosphate pathway in cancer cells (Anastasiou et al., 2011), but altered ribose production was not observed in *PKM2*$^{\Delta/\Delta}$ MEFs. Regardless of how pyruvate kinase influences nucleotide synthesis, these findings support the notion that independent of nutrient uptake, how nutrients are metabolized determines whether cells engage in proliferation.

EXPERIMENTAL PROCEDURES

All mouse studies were performed in accordance with institutional guidelines and approved by the MIT Committee on Animal Care.

Isolation and culture of primary mouse embryonic fibroblasts

Primary mouse embryonic fibroblasts (MEFs) were isolated and cultured using published methods (Springer et al., 2001). Embryos were isolated at E11.5 – E14.5 of gestation, and each embryo processed separately. MEFs were cultured in MEF medium (Dulbecco's Modified Eagle's Medium with 10% heat inactivated FBS, 1% streptomycin/penicillin, 1 mM glutamine, and 0.1 mM 2-mercaptoethanol) and plated at a density of 5×10^6 cells per 10 cm plate. Cells were split before reaching confluence and replated at 750,000 cells per 10 cm plate. 1 μM 4-hydroxytamoxifen in ethanol was used to induce recombination of *PKM2*^{fl} alleles. Cells starved of lysine were incubated in lysine-free DMEM and doubling time analyzed over 10 days.

Cell proliferation analysis

750,000 cells were seeded in triplicate in 10 cm plates, and cell counts obtained using a Cellometer Auto T4 Cell Counter (Nexcelom). Cells were replated at 70% confluence, counted, and reseeded at a density of 750,000 per 10 cm plate. Population doubling (PD) was calculated using the following formula:

$$PD = \frac{log\left(\frac{number\ of\ cells\ counted}{number\ of\ cells\ seeded}\right)}{log(2)} + previous\ PD.$$

When used, all metabolite supplements were added to MEF medium at a concentration of 250 μM.

Metabolite uptake and excretion

Conditioned medium was sampled after 72 h. Levels of glucose and lactate were measured using YSI 7100 Select Biochemistry Analyzer. The following equation was used to calculate metabolite consumption/excretion per 10^6 cells per hour (α):

$$\alpha = \frac{[metabolite]_{initial} - [metabolite]_{final}}{\frac{X_{initial}}{\mu} \cdot (e^{\mu \Delta t} - 1)}$$

where

$$\mu = \text{specific growth rate} = \frac{1}{t} \cdot ln\left(\frac{X_{final}}{X_{initial}}\right)$$

and *X* is cell number and *t* is time in hours. For μ of 0 (specific growth rate of 0), α was calculated using the following equation:

$$\alpha = \frac{[metabolite]_{initial} - [metabolite]_{final}}{X \cdot \Delta t}.$$

Metabolite extraction and analysis

For metabolite analysis using gas chromatography/mass spectrometry, cells were cultured for ~72 h in in glucose- and glutamine-free DMEM-based MEF media with dialyzed FBS and the appropriate tracer added. [U-$^{13}C_6$]glucose, [U-$^{13}C_5$]glutamine, and [5-^{13}C]glutamine were all from Cambridge Isotopes Laboratories, Inc.

Cell cycle analysis

Cells were fixed in ice cold ethanol at 4°C overnight, washed twice in PBS with 1% BSA, treated with RNase, and resuspended in propidium iodide buffer to a final concentration of 50 μg·ml^{-1}. Cells were analyzed on a Becton Dickinson FACScan flow

cytometer. To assay for new DNA synthesis, the Click-iT EdU Alexa Fluor 488 kit was used with 3 hour exposure of cells to 10 μM EdU (Invitrogen C35002), and imaged on a Nikon Eclipse TE2000-U microscope with a 4 second exposure time and analyzed using the ImageJ software. Cells were dual stained for DNA content and new DNA synthesis with the Click-iT EdU Alexa Fluor 488 Kit and FxCycle Violet Stain (Life Technologies F-10347), respectively, and analyzed on a BD FACSCanto II using FACS Diva software. Viability was assessed by propidium iodide dye exclusion using a BD FACScan flow cytometer.

Measurement of cell mass and volume

Dry mass of single cells was measured as previously described (Feijo Delgado et al., 2013). Briefly, cells were resuspended in 1x PBS and loaded into a 15x20 μm cross-section suspended microchannel resonator. The buoyant mass of each cell was measured first in 1x PBS and then in 1x D_2O-PBS. Each experiment was conducted for approximately 1.5 h at room temperature. For measurement of cell dry weight from batch culture, 10^6 cells were captured onto membrane filters, dried at 37°C for several days and weighed using an analytical balance. Weights of control membrane filters loaded only with PBS before drying was subtracted to obtain the weight of 10^6 cells. Cell volumes were measured using a Coulter counter.

DNA strand labeling

Cells were incubated in medium containing 100 μM CldU (Sigma Aldrich C6891) for 20 min, washed with PBS, and then incubated in medium containing 250 μM IdU (Sigma

Aldrich I7125) for 20 min. Following trypsinization, labeled cells were resuspended in PBS with tenfold excess of unlabeled cells and 2.5 µL were transferred to a glass slide with 7.5 µL of spreading buffer (200 mM Tris-HCl pH 7.5, 50 mM EDTA, .5% SDS). Slides were dried and fixed in cold 3:1 methanol:acetic acid for 2 min. Following a 30 min treatment with 2.5 N HCl to denature the DNA, slides were washed with PBS and blocked at 37 ºC with PBST + 2% BSA. The samples were then incubated at 37 ºC for 1 hr in PBST + 1% BSA containing primary antibodies to CldU (AbD Serotec OBT0030) and IdU (BD 347580), washed with PBST, and incubated at 37 ºC for 30 min in PBST + 1% BSA containing secondary antibodies conjugated to Cy3 (Jackson Immunochemicals 712-165-153) and Alexa Fluor 488 (Jackson Immunochemicals 715-545-151) with minimal cross-reactivity to mouse and rat IgG, respectively. Samples were imaged using the DeltaVision Elite imaging system (Applied Precision) and microscope (model IX-71; Olympus) with a 100x objective lens, and the CoolSNAP HQ2 camera (Photometrics).

Accession Number

Gene Expression Omnibus GSE60499.

SUPPLEMENTAL INFORMATION

Supplemental information includes seven figures, two tables, Supplemental Experimental Procedures, and the description of the flux model with the complete flux data provided as an Excel spreadsheet.

ACKNOWLEDGMENTS

This research was supported by the Department of Defense CDMRP Visionary Postdoctoral Award under award number (W81XWH-12-1-0466) to SYL. The work of SMF was supported by Marie Curie CIG, FWO-Odysseus II, Concern Foundation funding, and Bayer Healthcare Pharmaceuticals. This work was also supported by the Smith Family Foundation, the Burroughs Wellcome Fund, the Damon Runyon Cancer Research Foundation, the Stern family, the American Association for Cancer Research, and the National Cancer Institute including NIH 5P30CA1405141 and R01CA168653. The authors thank Gavin Reid and Julia Busik for access to their laboratories; Stephanie Yazinski for experimental advice; Alice Chen, Amy Liu, Olivia Czajkowski, Jordan Honeysett, Michael Monterey, Jon Rennhack, Eric Poliner, Blair Bullard, Christoph Benning, and the Koch Institute Swanson Biotechnology Center for technical assistance; Craig Thomas and Matthew Boxer for providing PKM2 activators; Christian Metallo, Eric Bell, Ben Olenchock, Caroline Lewis, Brian Fiske, Katie Mattaini, Shawn Davidson, Jared Mayers, Amelia Yu, and Zach Johnson for thoughtful discussions and comments on the manuscript.

REFERENCES

Abmayr, S.M., and Pavlath, G.K. (2012). Myoblast fusion: lessons from flies and mice. Development *139*, 641-656.

Aird, Katherine M., Zhang, G., Li, H., Tu, Z., Bitler, Benjamin G., Garipov, A., Wu, H., Wei, Z., Wagner, Stephan N., Herlyn, M.*, et al.* (2013). Suppression of Nucleotide Metabolism Underlies the Establishment and Maintenance of Oncogene-Induced Senescence. Cell Reports *3*, 1252-1265.

Anastasiou, D., Poulogiannis, G., Asara, J.M., Boxer, M.B., Jiang, J.-k., Shen, M., Bellinger, G., Sasaki, A.T., Locasale, J.W., Auld, D.S.*, et al.* (2011). Inhibition of Pyruvate Kinase M2 by Reactive Oxygen Species Contributes to Cellular Antioxidant Responses. Science *334*, 1278-1283.

Anastasiou, D., Yu, Y., Israelsen, W.J., Jiang, J.-K., Boxer, M.B., Hong, B.S., Tempel, W., Dimov, S., Shen, M., Jha, A.*, et al.* (2012). Pyruvate kinase M2 activators promote tetramer formation and suppress tumorigenesis. Nat Chem Biol *8*, 839-847.

Anglana, M., Apiou, F., Bensimon, A., and Debatisse, M. (2003). Dynamics of DNA Replication in Mammalian Somatic Cells: Nucleotide Pool Modulates Origin Choice and Interorigin Spacing. Cell *114*, 385-394.

Antoniewicz, M.R., Kelleher, J.K., and Stephanopoulos, G. (2007). Elementary metabolite units (EMU): a novel framework for modeling isotopic distributions. Metabolic engineering *9*, 68-86.

Bester, Assaf C., Roniger, M., Oren, Yifat S., Im, Michael M., Sarni, D., Chaoat, M., Bensimon, A., Zamir, G., Shewach, Donna S., and Kerem, B. (2011). Nucleotide Deficiency Promotes Genomic Instability in Early Stages of Cancer Development. Cell *145*, 435-446.

Bohnsack, B.L., and Hirschi, K.K. (2004). NUTRIENT REGULATION OF CELL CYCLE PROGRESSION. Annual Review of Nutrition *24*, 433-453.

Burg, T.P., Godin, M., Knudsen, S.M., Shen, W., Carlson, G., Foster, J.S., Babcock, K., and Manalis, S.R. (2007). Weighing of biomolecules, single cells and single nanoparticles in fluid. Nature *446*, 1066-1069.

Cairns, R.A., Harris, I.S., and Mak, T.W. (2011). Regulation of cancer cell metabolism. Nat Rev Cancer *11*, 85-95.

Campisi, J. (2011). Cellular senescence: putting the paradoxes in perspective. Current Opinion in Genetics & Development *21*, 107-112.

Castro, P., Giri, D., Lamb, D., and Ittmann, M. (2003). Cellular senescence in the pathogenesis of benign prostatic hyperplasia. The Prostate *55*, 30-38.

Chaneton, B., Hillmann, P., Zheng, L., Martin, A.C.L., Maddocks, O.D.K., Chokkathukalam, A., Coyle, J.E., Jankevics, A., Holding, F.P., Vousden, K.H.*, et al.* (2012). Serine is a natural ligand and allosteric activator of pyruvate kinase M2. Nature *491*, 458-462.

Christofk, H.R., Vander Heiden, M.G., Harris, M.H., Ramanathan, A., Gerszten, R.E., Wei, R., Fleming, M.D., Schreiber, S.L., and Cantley, L.C. (2008a). The M2 splice isoform of pyruvate kinase is important for cancer metabolism and tumour growth. Nature *452*, 230-233.

Christofk, H.R., Vander Heiden, M.G., Wu, N., Asara, J.M., and Cantley, L.C. (2008b). Pyruvate kinase M2 is a phosphotyrosine-binding protein. Nature *452*, 181-186.

Clower, C.V., Chatterjee, D., Wang, Z., Cantley, L.C., Vander Heiden, M.G., and Krainer, A.R. (2010). The alternative splicing repressors hnRNP A1/A2 and PTB influence pyruvate kinase isoform expression and cell metabolism. Proceedings of the National Academy of Sciences *107*, 1894-1899.

Cohen, A., Barankiewicz, J., Lederman, H.M., and Gelfand, E.W. (1983). Purine and pyrimidine metabolism in human T lymphocytes. Regulation of deoxyribonucleotide metabolism. Journal of Biological Chemistry *258*, 12334-12340.

Cunningham, John T., Moreno, Melissa V., Lodi, A., Ronen, Sabrina M., and Ruggero, D. (2014). Protein and Nucleotide Biosynthesis Are Coupled by a Single Rate-Limiting Enzyme, PRPS2, to Drive Cancer. Cell *157*, 1088-1103.

Decker, T., and Lohmann-Matthes, M.-L. (1988). A quick and simple method for the quantitation of lactate dehydrogenase release in measurements of cellular cytotoxicity and tumor necrosis factor (TNF) activity. Journal of Immunological Methods *115*, 61-69.

Dimri, G.P., Lee, X., Basile, G., Acosta, M., Scott, G., Roskelley, C., Medrano, E.E., Linskens, M., Rubelj, I., and Pereira-Smith, O. (1995). A biomarker that identifies senescent human cells in culture and in aging skin in vivo. Proceedings of the National Academy of Sciences *92*, 9363-9367.

Domingo, M., Einig, C., Eigenbrodt, E., and Reinacher, M. (1992). Immunohistological demonstration of pyruvate kinase isoenzyme type L in rat with monoclonal antibodies. Journal of Histochemistry & Cytochemistry *40*, 665-673.

Eigenbrodt, E., and Glossmann, H. (1980). Glycolysis one of the keys to cancer? Trends in pharmacological sciences *1*, 240-245.

Feijo Delgado, F., Cermak, N., Hecht, V.C., Son, S., Li, Y., Knudsen, S.M., Olcum, S., Higgins, J.M., Chen, J., Grover, W.H.*, et al.* (2013). Intracellular water exchange for measuring the dry mass, water mass and changes in chemical composition of living cells. PloS one *8*, e67590.

Fendt, S.-M., Bell, E.L., Keibler, M.A., Davidson, S.M., Wirth, G.J., Fiske, B., Mayers, J.R., Schwab, M., Bellinger, G., Csibi, A.*, et al.* (2013a). Metformin Decreases Glucose Oxidation and Increases the Dependency of Prostate Cancer Cells on Reductive Glutamine Metabolism. Cancer Research *73*, 4429-4438.

Fendt, S.-M., Bell, E.L., Keibler, M.A., Olenchock, B.A., Mayers, J.R., Wasylenko, T.M., Vokes, N.I., Guarente, L., Heiden, M.G.V., and Stephanopoulos, G. (2013b). Reductive glutamine metabolism is a function of the α-ketoglutarate to citrate ratio in cells. Nat Commun *4*.

Foster, D.A., Yellen, P., Xu, L., and Saqcena, M. (2010). Regulation of G1 Cell Cycle Progression Distinguishing the Restriction Point from a Nutrient-Sensing Cell Growth Checkpoint (s). Genes & cancer *1*, 1124-1131.

Gangjee, A., Jain, H.D., and Kurup, S. (2007). Recent Advances in Classical and Non-Classical Antifolates as Antitumor and Antiopportunistic Infection Agents: Part I. Anti-Cancer Agents in Medicinal Chemistry- Anti-Cancer Agents) *7*, 524-542.

Gao, X., Wang, H., Yang, Jenny J., Liu, X., and Liu, Z.-R. (2012). Pyruvate Kinase M2 Regulates Gene Transcription by Acting as a Protein Kinase. Molecular cell *45*, 598-609.

Green, H., and Kehinde, O. (1974). Sublines of mouse 3T3 cells that accumulate lipid. Cell *1*, 113-116.

Gui, D.Y., Lewis, C.A., and Vander Heiden, M.G. (2013). Allosteric Regulation of PKM2 Allows Cellular Adaptation to Different Physiological States. Sci. Signal. *6*, 7.

Hacker, H.J., Steinberg, P., and Bannasch, P. (1998). Pyruvate kinase isoenzyme shift from L-type to M2-type is a late event in hepatocarcinogenesis induced in rats by a choline-deficient/DL-ethionine-supplemented diet. Carcinogenesis *19*, 99-107.

Hanahan, D., and Weinberg, Robert A. (2011). Hallmarks of Cancer: The Next Generation. Cell *144*, 646-674.

Harrap, K.R., Taylor, G.A., and Browman, G.P. (1977). Enhancement of the therapeutic effectiveness of methotrexate and protection of normal proliferating tissues with purines and pyrimidines. Chemico-Biological Interactions *18*, 119-128.

Hawser, S., Lociuro, S., and Islam, K. (2006). Dihydrofolate reductase inhibitors as antibacterial agents. Biochemical Pharmacology *71*, 941-948.

Hryniuk, W.M. (1975). The Mechanism of Action of Methotrexate in Cultured L5178Y Leukemia Cells. Cancer Research *35*, 1085-1092.

Hryniuk, W.M., Brox, L.W., Henderson, J.F., and Tamaoki, T. (1975). Consequences of Methotrexate Inhibition of Purine Biosynthesis in L5178Y Cells. Cancer Research *35*, 1427-1432.

Illg, D., and Pette, D. (1979). Turnover Rates of Hexokinase I, Phosphofructokinase, Pyruvate Kinase and Creatine Kinase in Slow-Twitch Soleus Muscle and Heart of the Rabbit. European Journal of Biochemistry *97*, 267-273.

Imamura, K., Noguchi, T., and Tanaka, T. (1986). In Markers of Human Neuroectodermal Tumors, G.E.J. Staal, and C.W.M. van Veelen, eds. (Boca Raton, FL: CRC Press), pp. 191-222.

Imamura, K., and Tanaka, T. (1982). Pyruvate kinase isozymes from rat. In Methods in Enzymology, A.W. Willis, ed. (Academic Press), pp. 150-165.

Israelsen, William J., Dayton, Talya L., Davidson, Shawn M., Fiske, Brian P., Hosios, Aaron M., Bellinger, G., Li, J., Yu, Y., Sasaki, M., Horner, James W*., et al.* (2013). PKM2 Isoform-Specific Deletion Reveals a Differential Requirement for Pyruvate Kinase in Tumor Cells. Cell *155*, 397-409.

Jiang, Y., Li, X., Yang, W., Hawke, David H., Zheng, Y., Xia, Y., Aldape, K., Wei, C., Guo, F., Chen, Y*., et al.* (2014). PKM2 Regulates Chromosome Segregation and Mitosis Progression of Tumor Cells. Molecular cell *53*, 75-87.

Johnston, G.C., Pringle, J.R., and Hartwell, L.H. (1977). Coordination of growth with cell division in the yeast Saccharomyces cerevisiae. Experimental Cell Research *105*, 79-98.

Kamphorst, J.J., Cross, J.R., Fan, J., de Stanchina, E., Mathew, R., White, E.P., Thompson, C.B., and Rabinowitz, J.D. (2013). Hypoxic and Ras-transformed cells support growth by scavenging unsaturated fatty acids from lysophospholipids. Proceedings of the National Academy of Sciences *110*, 8882-8887.

Keller, Kirstie E., Doctor, Zainab M., Dwyer, Zachary W., and Lee, Y.-S. (2014). SAICAR Induces Protein Kinase Activity of PKM2 that Is Necessary for Sustained Proliferative Signaling of Cancer Cells. Molecular cell *53*, 700-709.

Keller, K.E., Tan, I.S., and Lee, Y.-S. (2012). SAICAR Stimulates Pyruvate Kinase Isoform M2 and Promotes Cancer Cell Survival in Glucose-Limited Conditions. Science *338*, 1069-1072.

Koppenol, W.H., Bounds, P.L., and Dang, C.V. (2011). Otto Warburg's contributions to current concepts of cancer metabolism. Nat Rev Cancer *11*, 325-337.

Kuilman, T., Michaloglou, C., Mooi, W.J., and Peeper, D.S. (2010). The essence of senescence. Genes & Development *24*, 2463-2479.

Kwon, Y.K., Higgins, M.B., and Rabinowitz, J.D. (2010). Antifolate-Induced Depletion of Intracellular Glycine and Purines Inhibits Thymineless Death in E. coli. ACS Chemical Biology *5*, 787-795.

Laliberté, J., Yee, A., Xiong, Y., and Mitchell, B.S. (1998). Effects of Guanine Nucleotide Depletion on Cell Cycle Progression in Human T Lymphocytes. Blood *91*, 2896-2904.

Lunt, S.Y., and Vander Heiden, M.G. (2011). Aerobic glycolysis: meeting the metabolic requirements of cell proliferation. Annu Rev Cell Dev Biol *27*, 441-464.

Luo, W., Hu, H., Chang, R., Zhong, J., Knabel, M., O'Meally, R., Cole, Robert N., Pandey, A., and Semenza, Gregg L. (2011). Pyruvate Kinase M2 Is a PHD3-Stimulated Coactivator for Hypoxia-Inducible Factor 1. Cell *145*, 732-744.

Lv, L., Li, D., Zhao, D., Lin, R., Chu, Y., Zhang, H., Zha, Z., Liu, Y., Li, Z., Xu, Y.*, et al.* (2011). Acetylation Targets the M2 Isoform of Pyruvate Kinase for Degradation through Chaperone-Mediated Autophagy and Promotes Tumor Growth. Molecular cell *42*, 719-730.

Mazurek, S. (2011). Pyruvate kinase type M2: A key regulator of the metabolic budget system in tumor cells. The International Journal of Biochemistry & Cell Biology *43*, 969-980.

Messina, E., Gazzaniga, P., Micheli, V., Guaglianone, M.R., Barbato, S., Morrone, S., Frati, L., Aglianò, A.M., and Giacomello, A. (2004). Guanine nucleotide depletion triggers cell cycle arrest and apoptosis in human neuroblastoma cell lines. International Journal of Cancer *108*, 812-817.

Metallo, C.M., Gameiro, P.A., Bell, E.L., Mattaini, K.R., Yang, J., Hiller, K., Jewell, C.M., Johnson, Z.R., Irvine, D.J., Guarente, L.*, et al.* (2012). Reductive glutamine metabolism by IDH1 mediates lipogenesis under hypoxia. Nature *481*, 380-384.

Meuth, M. (1989). The molecular basis of mutations induced by deoxyribonucleoside triphosphate pool imbalances in mammalian cells. Experimental Cell Research *181*, 305-316.

Montagne, J., Stewart, M.J., Stocker, H., Hafen, E., Kozma, S.C., and Thomas, G. (1999). Drosophila S6 Kinase: A Regulator of Cell Size. Science *285*, 2126-2129.

Nicoletti, I., Migliorati, G., Pagliacci, M.C., Grignani, F., and Riccardi, C. (1991). A rapid and simple method for measuring thymocyte apoptosis by propidium iodide staining and flow cytometry. Journal of Immunological Methods *139*, 271-279.

Noguchi, T., Inoue, H., and Tanaka, T. (1986). The M1- and M2-type isozymes of rat pyruvate kinase are produced from the same gene by alternative RNA splicing. Journal of Biological Chemistry *261*, 13807-13812.

Noguchi, T., Yamada, K., Inoue, H., Matsuda, T., and Tanaka, T. (1987). The L- and R-type isozymes of rat pyruvate kinase are produced from a single gene by use of different promoters. Journal of Biological Chemistry *262*, 14366-14371.

Odell, A., Askham, J., Whibley, C., and Hollstein, M. (2010). How to become immortal: let MEFs count the ways. Aging *2*, 160-165.

Reaves, M.L., Young, B.D., Hosios, A.M., Xu, Y.-F., and Rabinowitz, J.D. (2013). Pyrimidine homeostasis is accomplished by directed overflow metabolism. Nature *500*, 237-241.

Reichard, P. (1988). Interactions Between Deoxyribonucleotide and DNA Synthesis. Annual Review of Biochemistry *57*, 349-374.

Russell, T.R., and Ho, R. (1976). Conversion of 3T3 fibroblasts into adipose cells: triggering of differentiation by prostaglandin F2alpha and 1-methyl-3-isobutyl xanthine. Proceedings of the National Academy of Sciences *73*, 4516-4520.

Springer, M.L., Rando, T.A., and Blau, H.M. (2001). Gene Delivery to Muscle. In Current Protocols in Human Genetics (John Wiley & Sons, Inc.).

Steinberg, P., Klingelhöffer, A., Schäfer, A., Wüst, G., Weiße, G., Oesch, F., and Eigenbrodt, E. (1999). Expression of pyruvate kinase M2 in preneoplastic hepatic foci of N-nitrosomorpholine-treated rats. Virchows Archiv *434*, 213-220.

Tattersall, M.H.N., Jackson, R.C., Jackson, S.T.M., and Harrap, K.R. (1974). Factors determining cell sensitivity to methotrexate: Studies of folate and deoxyribonucleoside triphosphate pools in five mammalian cell lines. European Journal of Cancer (1965) *10*, 819-826.

Tu, B.P., Kudlicki, A., Rowicka, M., and McKnight, S.L. (2005). Logic of the Yeast Metabolic Cycle: Temporal Compartmentalization of Cellular Processes. Science *310*, 1152-1158.

Turka, L.A., Dayton, J., Sinclair, G., Thompson, C.B., and Mitchell, B.S. (1991). Guanine ribonucleotide depletion inhibits T cell activation. Mechanism of action of the immunosuppressive drug mizoribine. The Journal of Clinical Investigation *87*, 940-948.

van der Loo, B., Fenton, M.J., and Erusalimsky, J.D. (1998). Cytochemical Detection of a Senescence-Associated β-Galactosidase in Endothelial and Smooth Muscle Cells from Human and Rabbit Blood Vessels. Experimental Cell Research *241*, 309-315.

Van Veelen, C.W.M., Verbiest, H., Staal, G.E.J., and Vlug, A.M.C. (1977). ALANINE INHIBITION OF PYRUVATE KINASE IN GLIOMAS AND MENINGIOMAS: A DIAGNOSTIC TOOL IN SURGERY FOR GLIOMAS? The Lancet *310*, 384-385.

Wakelam, M.J. (1985). The fusion of myoblasts. Biochem. J. *228*, 1-12.

Ward, Patrick S., and Thompson, Craig B. (2012). Metabolic Reprogramming: A Cancer Hallmark Even Warburg Did Not Anticipate. Cancer Cell *21*, 297-308.

Witherspoon, M., Chen, Q., Kopelovich, L., Gross, S.S., and Lipkin, S.M. (2013). Unbiased Metabolite Profiling Indicates That a Diminished Thymidine Pool Is the Underlying Mechanism of Colon Cancer Chemoprevention by Alpha-Difluoromethylornithine. Cancer Discovery *3*, 1072-1081.

Yamada, K., and Noguchi, T. (1995). Alteration of isozyme gene expression during cell differentiation and oncogenesis. Nihon Rinsho *53*, 1112-1118.

Yamada, K., and Noguchi, T. (1999). Regulation of Pyruvate Kinase M Gene Expression. Biochemical and Biophysical Research Communications *256*, 257-262.

Yang, W., Xia, Y., Hawke, D., Li, X., Liang, J., Xing, D., Aldape, K., Hunter, T., Alfred Yung, W.K., and Lu, Z. (2012a). PKM2 Phosphorylates Histone H3 and Promotes Gene Transcription and Tumorigenesis. Cell *150*, 685-696.

Yang, W., Xia, Y., Ji, H., Zheng, Y., Liang, J., Huang, W., Gao, X., Aldape, K., and Lu, Z. (2011). Nuclear PKM2 regulates β-catenin transactivation upon EGFR activation. Nature *478*, 118-122.

Yang, W., Zheng, Y., Xia, Y., Ji, H., Chen, X., Guo, F., Lyssiotis, C.A., Aldape, K., Cantley, L.C., and Lu, Z. (2012b). ERK1/2-dependent phosphorylation and nuclear translocation of PKM2 promotes the Warburg effect. Nat Cell Biol *14*, 1295-1304.

Yee, J.C., Jacob, N.M., Jayapal, K.P., Kok, Y.-J., Philp, R., Griffin, T.J., and Hu, W.-S. (2010). Global assessment of protein turnover in recombinant antibody producing myeloma cells. Journal of Biotechnology *148*, 182-193.

Young, J.D., Walther, J.L., Antoniewicz, M.R., Yoo, H., and Stephanopoulos, G. (2008). An elementary metabolite unit (EMU) based method of isotopically nonstationary flux analysis. Biotechnol Bioeng *99*, 686-699.

FIGURE LEGENDS

Figure 1. PKM2 deletion with PKM1 expression results in proliferation arrest.

(A) The effect of 4-OHT treatment on pyruvate kinase isoform expression in *PKM2*$^{fl/fl}$ *Cre-ER* MEFs was assessed by Western blot analysis. *PKM2*$^{fl/fl}$ *Cre-ER* MEFs were treated with 4-OHT (*PKM2*$^{\Delta/\Delta}$ *Cre-ER*) or vehicle (*PKM2*$^{fl/fl}$ *Cre-ER)* for the indicated number of days. Muscle or H1299 cancer cell lysate were included as control samples that express only PKM1 or PKM2, respectively.

(B) Proliferation of *PKM2*$^{fl/fl}$ *Cre-ER* MEFs following vehicle (*PKM2*$^{fl/fl}$ *Cre-ER)* or 4-OHT (*PKM2*$^{\Delta/\Delta}$ *Cre-ER)* treatment was assessed by counting cell numbers as shown.

(C) Proliferation of Cre negative *PKM2*$^{fl/fl}$ MEFs treated with vehicle or 4-OHT was assessed by counting cell numbers as shown.

(D) Western blot analysis of MEFs generated from *PKM2*$^{fl/+}$ *Cre-ER* mice. 4-OHT treatment results in *PKM2*$^{fl/\Delta}$ MEFs that express both PKM2 and PKM1 protein. Western blot analysis of 100 ng of recombinant PKM1 or PKM2 (rPKM1, rPKM2) are included as controls.

(E) Proliferation of *PKM2*$^{fl/+}$ *Cre-ER* MEFs treated with vehicle (*PKM2*$^{fl/+}$) or with 4-OHT (*PKM2*$^{\Delta/+}$) was assessed by counting cell numbers as shown.

(F) Proliferation of wildtype MEFs treated with vehicle or 1 μM of PKM2 activator TEPP-46 was assessed by counting cell numbers over time as shown.

All data are displayed as means ± SEM, n=3.

See also **Figure S1**.

Figure 2. *PKM2*$^{\Delta/\Delta}$ cells undergo cell cycle arrest.

(A) Quantification of cell viability by propidium iodide staining after treatment of *PKM2*$^{fl/fl}$ MEFs with vehicle (*PKM2*$^{fl/fl}$) or 4-OHT (*PKM2*$^{\Delta/\Delta}$). Data are displayed as means ± SEM, n=3.

(B) Classical cell senescence was assayed by acid stable β-galactosidase activity. The top panels (labeled Early passage) assess acid stable β-galactosidase activity in *PKM2*$^{fl/fl}$ and *PKM2*$^{\Delta/\Delta}$ MEFs 9 days after vehicle or 4-OHT treatment, respectively. Bottom panels (labeled Late passage) assess acid stable β-galactosidase activity in *PKM2*$^{fl/fl}$ and *PKM2*$^{\Delta/\Delta}$ MEFs after 12 days in culture. The *PKM2*$^{fl/fl}$ MEFs had undergone proliferation arrest at this time point.

(C) Population doublings over 12 days for myoblasts isolated from three different *PKM2*$^{fl/fl}$ *Cre-ER* mice that were treated with vehicle (*PKM2*$^{fl/fl}$) or 4-OHT (*PKM2*$^{\Delta/\Delta}$). Data are displayed as means ± SEM, n=3.

(D) Images of myoblasts generated from *PKM2*$^{fl/fl}$ *Cre-ER* mice 9 days after treatment with vehicle (*PKM2*$^{fl/fl}$) or 4-OHT (*PKM2*$^{\Delta/\Delta}$) are shown. *PKM2*$^{fl/fl}$ myoblasts induced to differentiate by culture in low-serum for 9 days are also presented (right panel).

(E) EdU uptake of *PKM2*$^{fl/fl}$ and *PKM2*$^{\Delta/\Delta}$ MEFs was measured in *PKM2*$^{fl/fl}$ *Cre-ER* MEFs 7 days after vehicle or 4-OHT treatment. Data are displayed as means ± SEM, n=3.

(F) DNA content was assessed using propidium iodide staining and flow cytometry in *PKM2*$^{fl/fl}$ and *PKM2*$^{\Delta/\Delta}$ MEFs 7 days after *PKM2*$^{fl/fl}$ *Cre-ER* MEFs were treated with vehicle or 4-OHT.

(G) DNA content was assessed following dual staining with FxCycle Violet and EdU using flow cytometry in *PKM2*$^{fl/fl}$ and *PKM2*$^{\Delta/\Delta}$ MEFs 7 days after *PKM2*$^{fl/fl}$ *Cre-ER* MEFs were treated with vehicle or 4-OHT.

See also **Figure S2**.

Figure 3. *PKM2*$^{\Delta/\Delta}$ cells remain metabolically active and are larger than *PKM2*$^{fl/fl}$ cells.

(A) Glucose uptake rates; **(B)** lactate excretion rates; **(C)** the relative production of ^{14}C-labeled CO_2 from uniformly ^{14}C-labeled glucose; **(D)** average cell volumes; **(E)** total protein content; and **(F)** single cell dry mass of *PKM2*$^{fl/fl}$ and *PKM2*$^{\Delta/\Delta}$ MEFs 7 days after

treatment of *PKM2*$^{fl/fl}$ MEFs with vehicle or 4-OHT. All data are displayed as means ± SEM, n=3 (*p < 0.0001).

See also **Figure S3**.

Figure 4. Pyruvate kinase isoform expression affects the use of specific metabolic pathways.

(A) Labeling of intracellular metabolites with [U-^{13}C]glucose or **(B)** [U-^{13}C]glutamine was measured using mass spectrometry in *PKM2*$^{fl/fl}$ and *PKM2*$^{\Delta/\Delta}$ MEFs 7 days after *PKM2*$^{fl/fl}$ *Cre-ER* MEFs were treated with vehicle or 4-OHT. Complete isotopomer distributions used to calculate these values are included in **Table S1**. The y-axis for all graphs in **(A)** is the calculated percent total glucose contribution (Fendt et al., 2013a).

See also **Figure S4**.

Figure 5. Nucleotide deficiency is limiting for proliferation of *PKM2*$^{\Delta/\Delta}$ MEFs.

(A) Pool sizes of intracellular nucleotides in *PKM2*$^{fl/fl}$ and *PKM2*$^{\Delta/\Delta}$ MEFs were measured 7 days after *PKM2*$^{fl/fl}$ *Cre-ER* MEFs were treated with vehicle or 4-OHT. Pool sizes of intracellular nucleotides in *PKM2*$^{\Delta/\Delta}$ MEFs supplemented with 250 μM thymine were also measured 7 days after 4-OHT treatment. Data are displayed as means ± SEM, n=4.

(B) Dynamic labeling of intracellular metabolites with [U-^{13}C]glucose and [U-^{13}C]glutamine was measured using mass spectrometry in *PKM2*$^{fl/fl}$ and *PKM2*$^{\Delta/\Delta}$ MEFs 7 days after *PKM2*$^{fl/fl}$ *Cre-ER* MEFs were treated with vehicle or 4-OHT. The complete isotopomer distributions for all measurements are included in **Table S2**.

(C) Metabolic fluxes of central carbon metabolism in *PKM2*$^{fl/fl}$ and *PKM2*$^{\Delta/\Delta}$ MEFs. Fluxes were modeled based on dynamic and steady state [U-^{13}C]glucose and [U-^{13}C]glutamine labeling data. With the exception of NTP and lactate, biomass and extraction fluxes are not depicted (see supplement for complete flux model). Significant differences (>40%, based on 95% confidence interval) between fluxes of PKM2$^{fl/fl}$ and PKM2$^{\Delta/\Delta}$ MEFs are highlighted in grey.

See also **Figure S5**, **Supplemental Experimental Procedures**, and **^{13}C-Metabolic flux analysis model**.

Figure 6. Genome-scale gene expression analysis reveals no correlation between gene expression and proliferation arrest of *PKM2*$^{\Delta/\Delta}$ cells.

(A) Unsupervised hierarchical clustering of *PKM2*$^{fl/fl}$ and *PKM2*$^{\Delta/\Delta}$ MEF expression profiles. RNA was isolated from *PKM2*$^{fl/fl}$ and *PKM2*$^{\Delta/\Delta}$ MEFs 7 days after *PKM2*$^{fl/fl}$ *Cre-ER* MEFs were treated with vehicle or 4-OHT. MEFs were generated from two independent *PKM2*$^{fl/fl}$ *Cre-ER* MEFs. RNA was analyzed using an Affymetrix GeneChip Mouse Gene 1.0 ST array.

(B) Unsupervised hierarchical clustering of *PKM2*$^{fl/fl}$ and *PKM2*$^{\Delta/\Delta}$ MEF expression profiles for genes involved in nucleotide metabolism.

See also **Figure S6**.

Figure 7. Thymine supplementation restores proliferation of *PKM2*$^{\Delta/\Delta}$ MEFs.

(A) Population doublings over 10 days of *PKM2*$^{fl/fl}$ and *PKM2*$^{\Delta/\Delta}$ MEFs were measured with or without the indicated metabolites supplemented in the media at a concentration of 250 μM. Data are displayed as means ± SEM, n=3. *Population doubling is statistically significant ($p < 0.05$) when compared to the population doubling of *PKM2*$^{\Delta/\Delta}$ MEFs without any supplements.

(B) Three representative images of DNA strands incorporating CldU (red) and IdU (green) from *PKM2*$^{fl/fl}$ and *PKM2*$^{\Delta/\Delta}$ MEFs five days after *PKM2*$^{fl/fl}$ *Cre-ER* MEFs were treated with vehicle or 4-OHT are shown; scale bar = 15 μm.

(C) Quantitation of the percentage of DNA strands incorporating both CldU and IdU is shown. For this analysis 237 strands from *PKM2*$^{fl/fl}$ MEFs and 54 strands from *PKM2*$^{\Delta/\Delta}$ MEFs prepared as described in (B) were evaluated.

See also **Figure S7**.

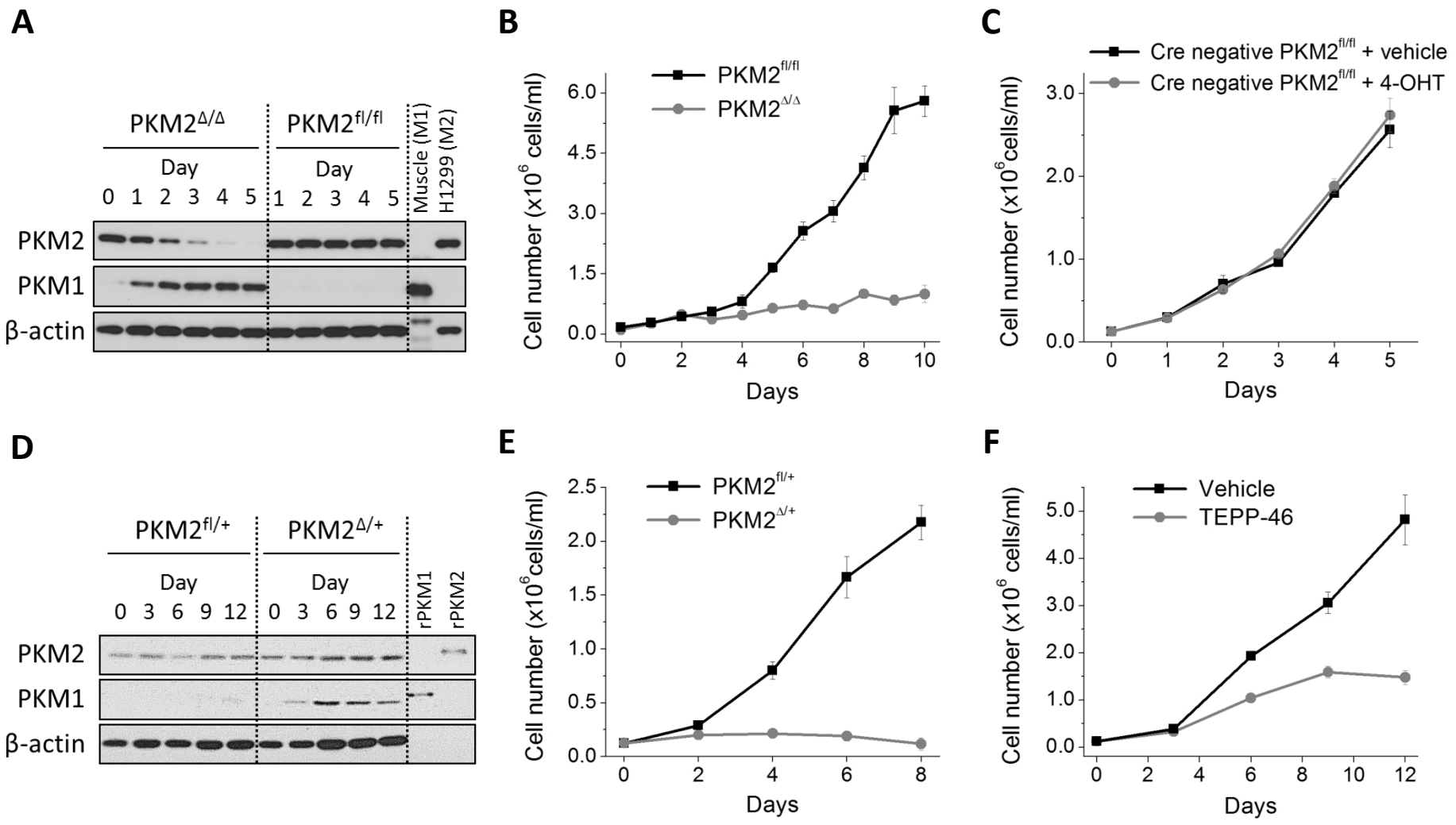

FIGURE 1 – Lunt *et al.*

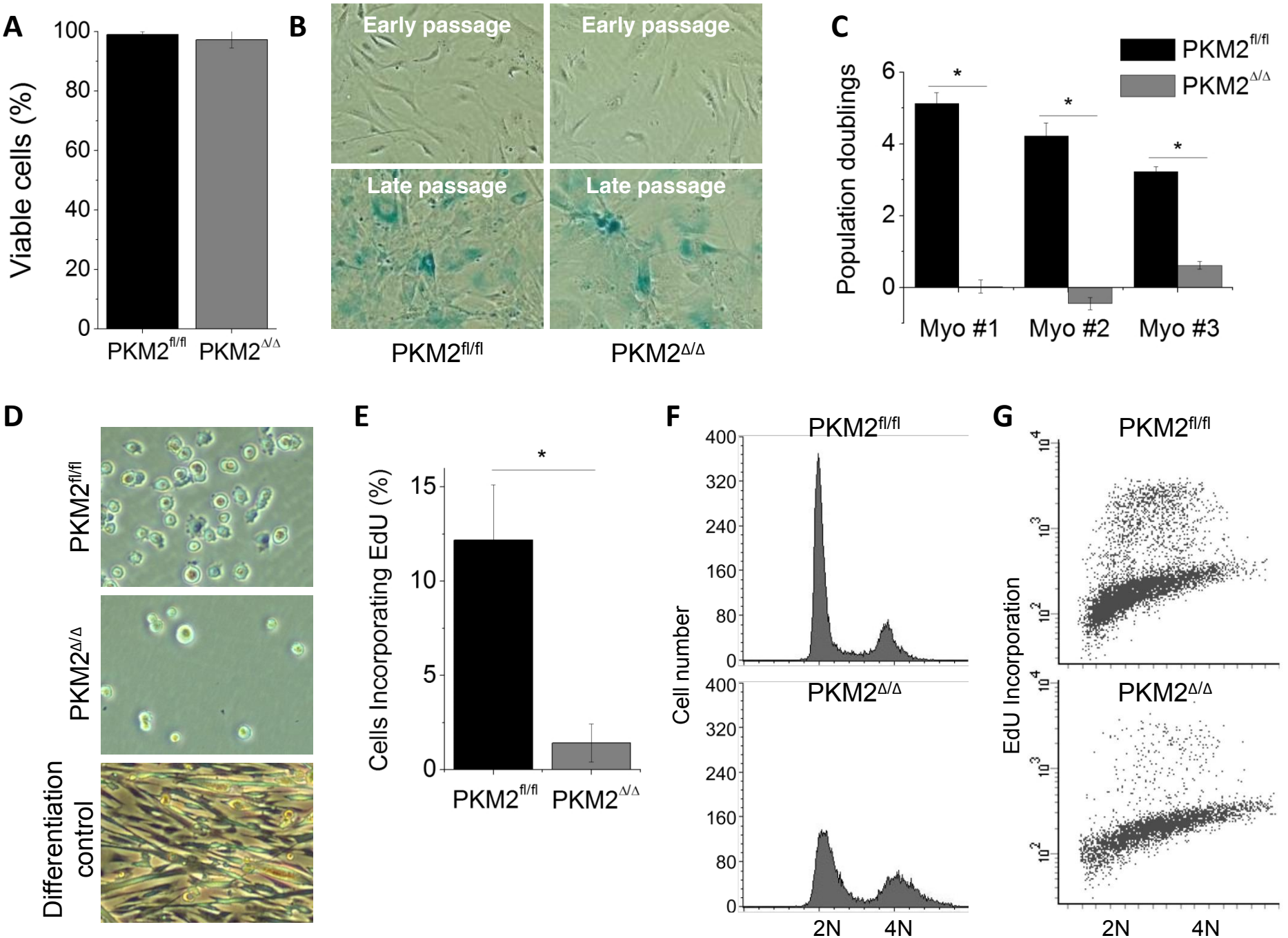

FIGURE 2 – Lunt *et al.*

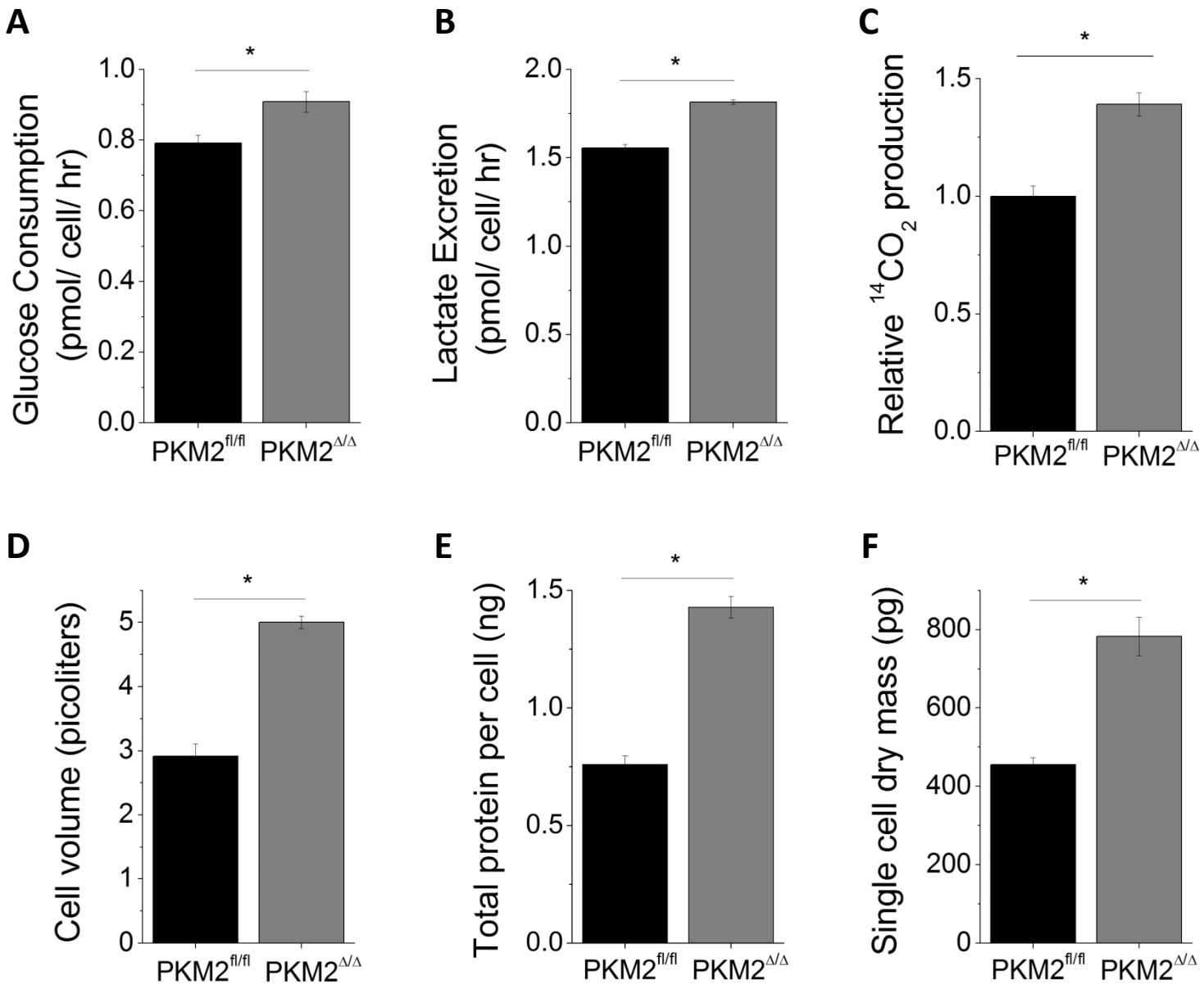

FIGURE 3 – Lunt *et al.*

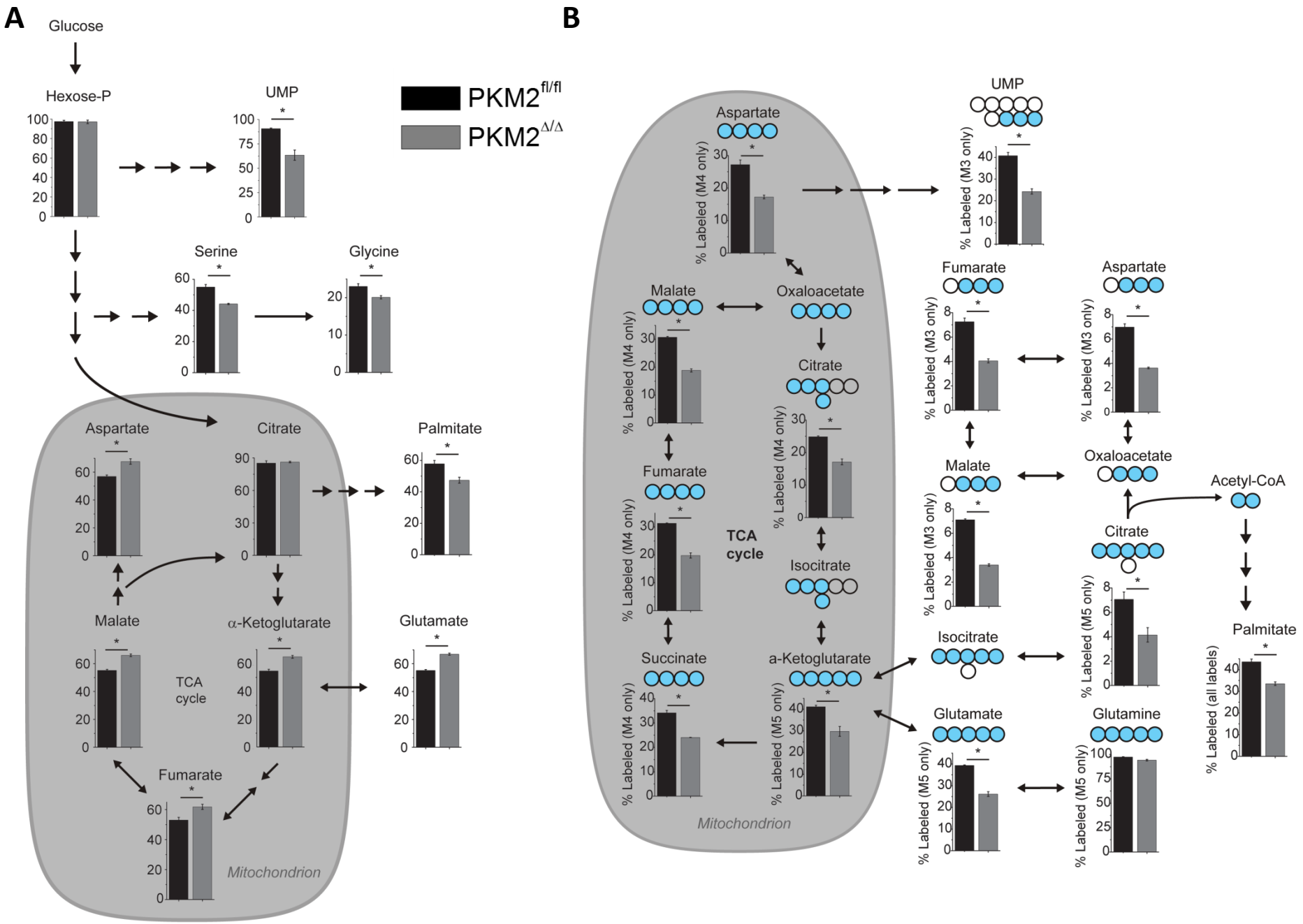

FIGURE 4 – Lunt *et al.*

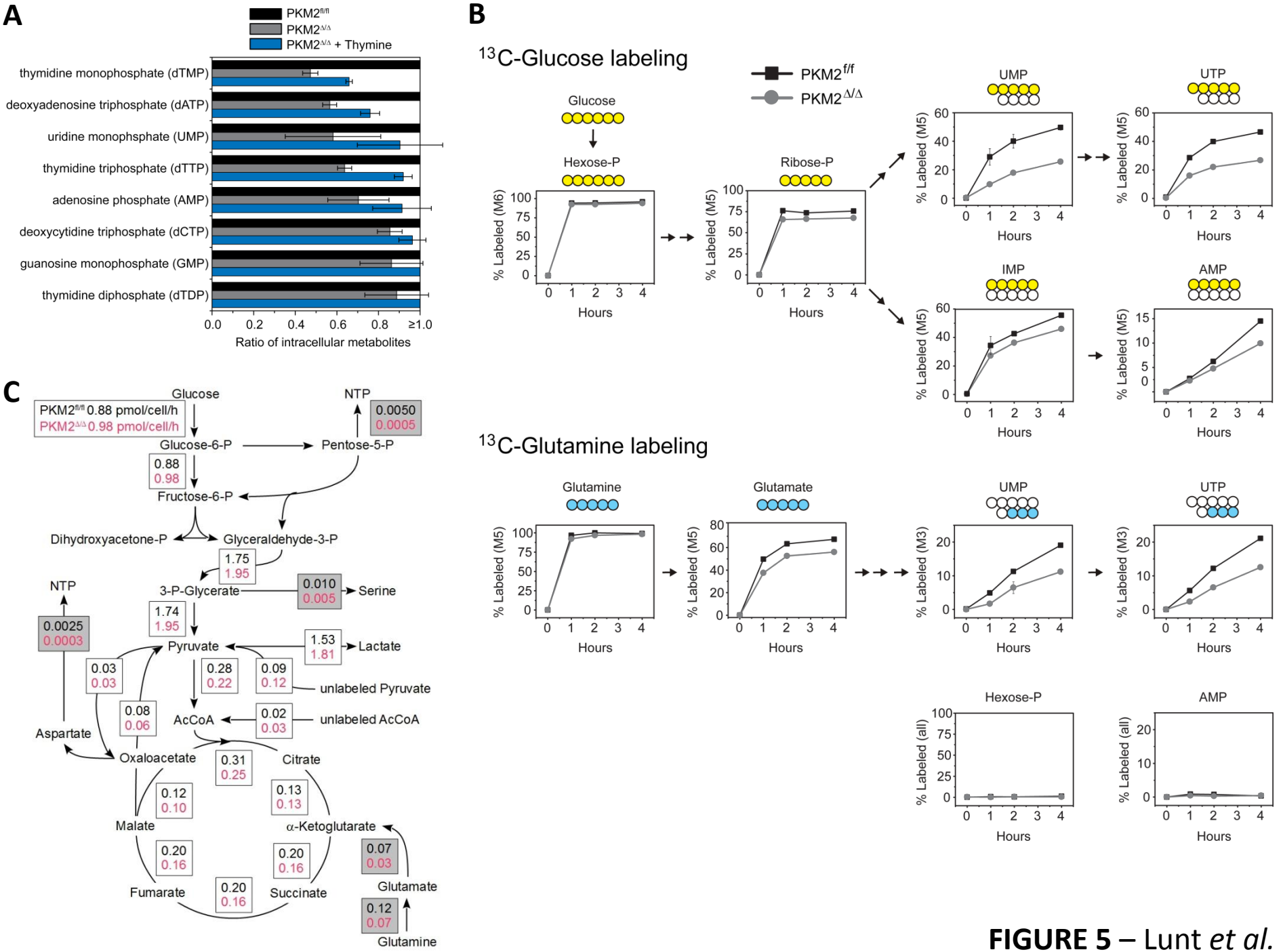

FIGURE 5 – Lunt *et al.*

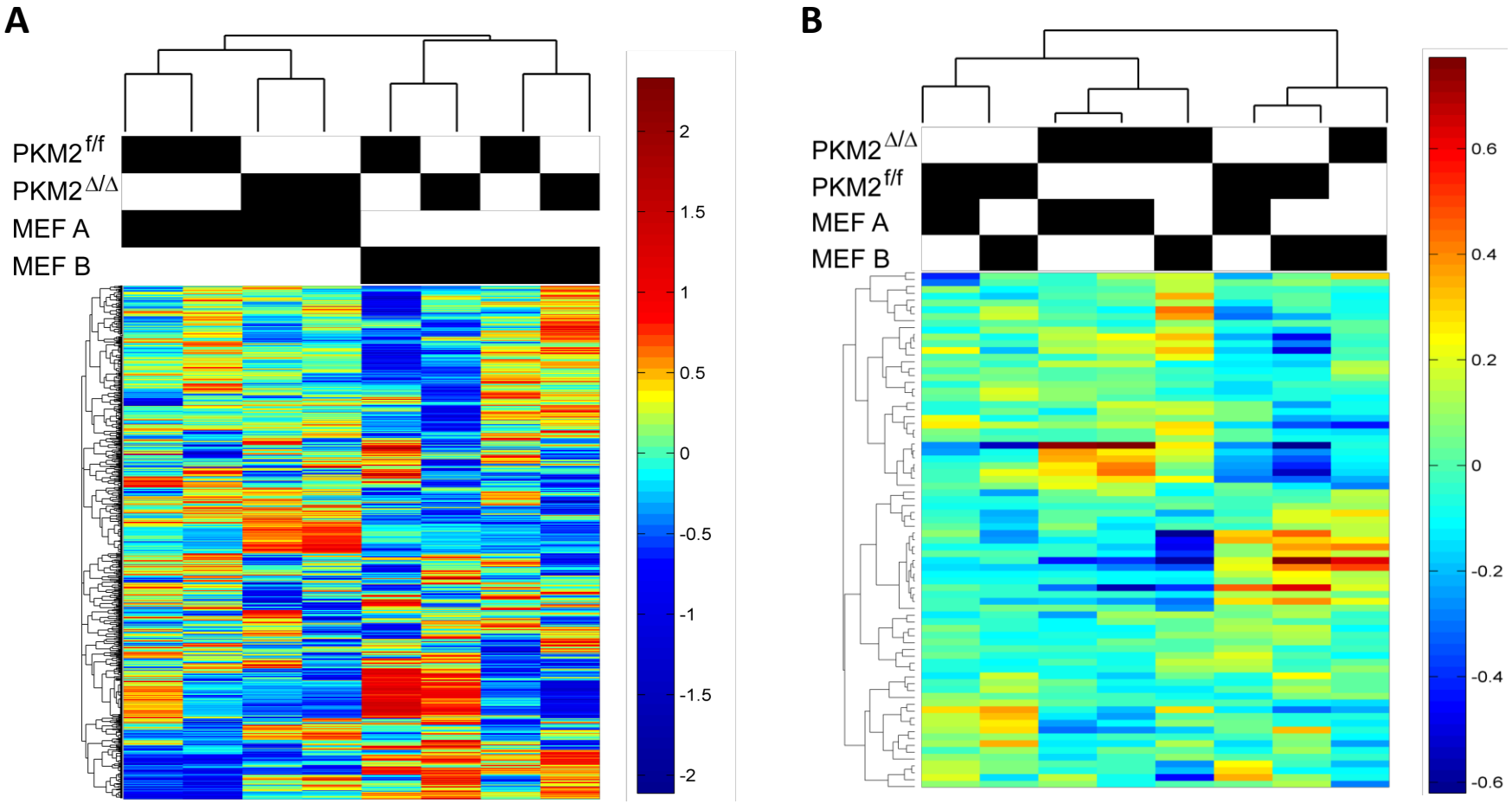

FIGURE 6 – Lunt *et al.*

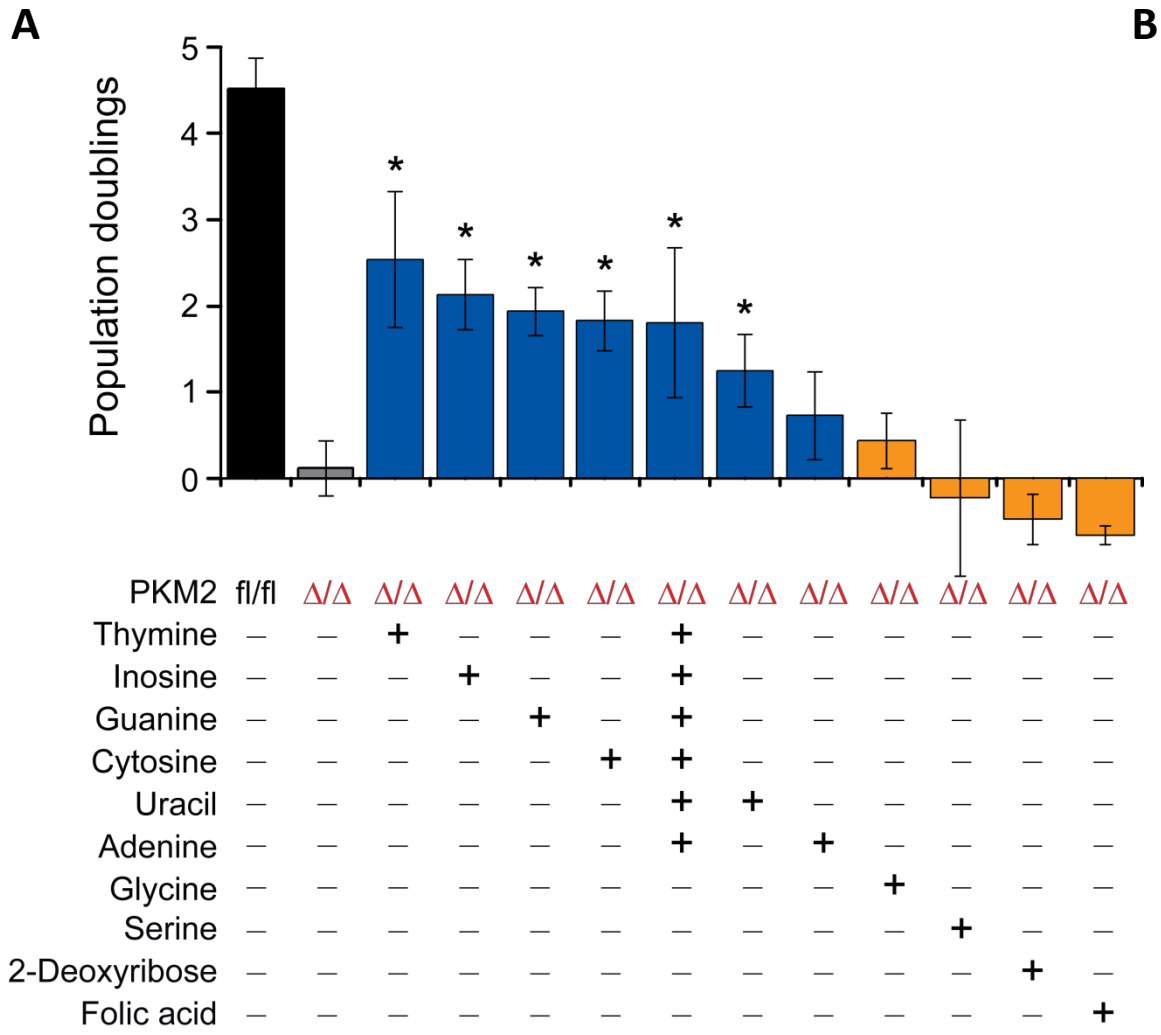

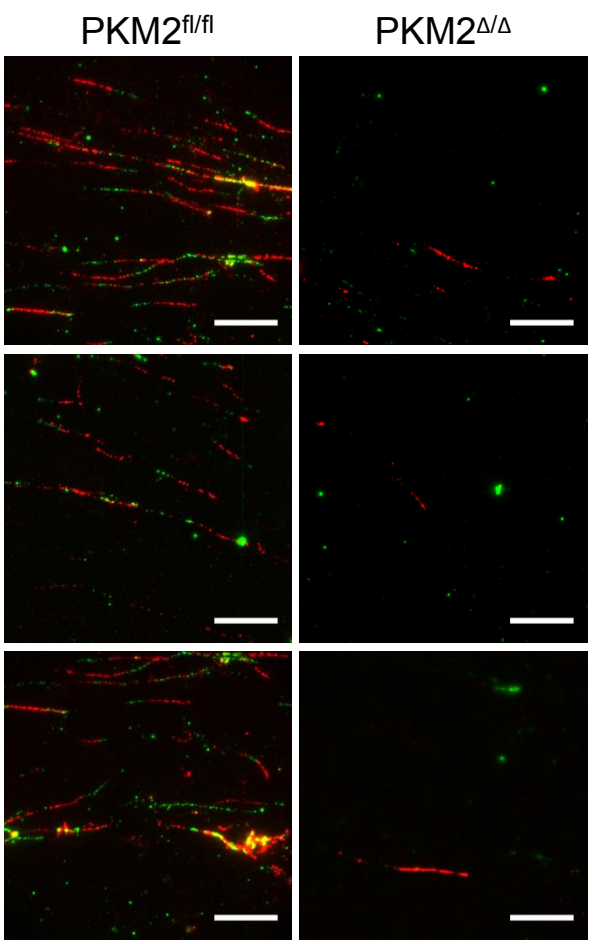

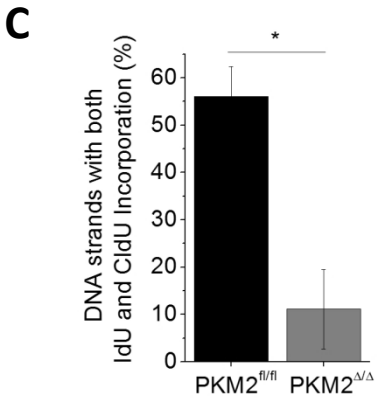

FIGURE 7 – Lunt *et al.*

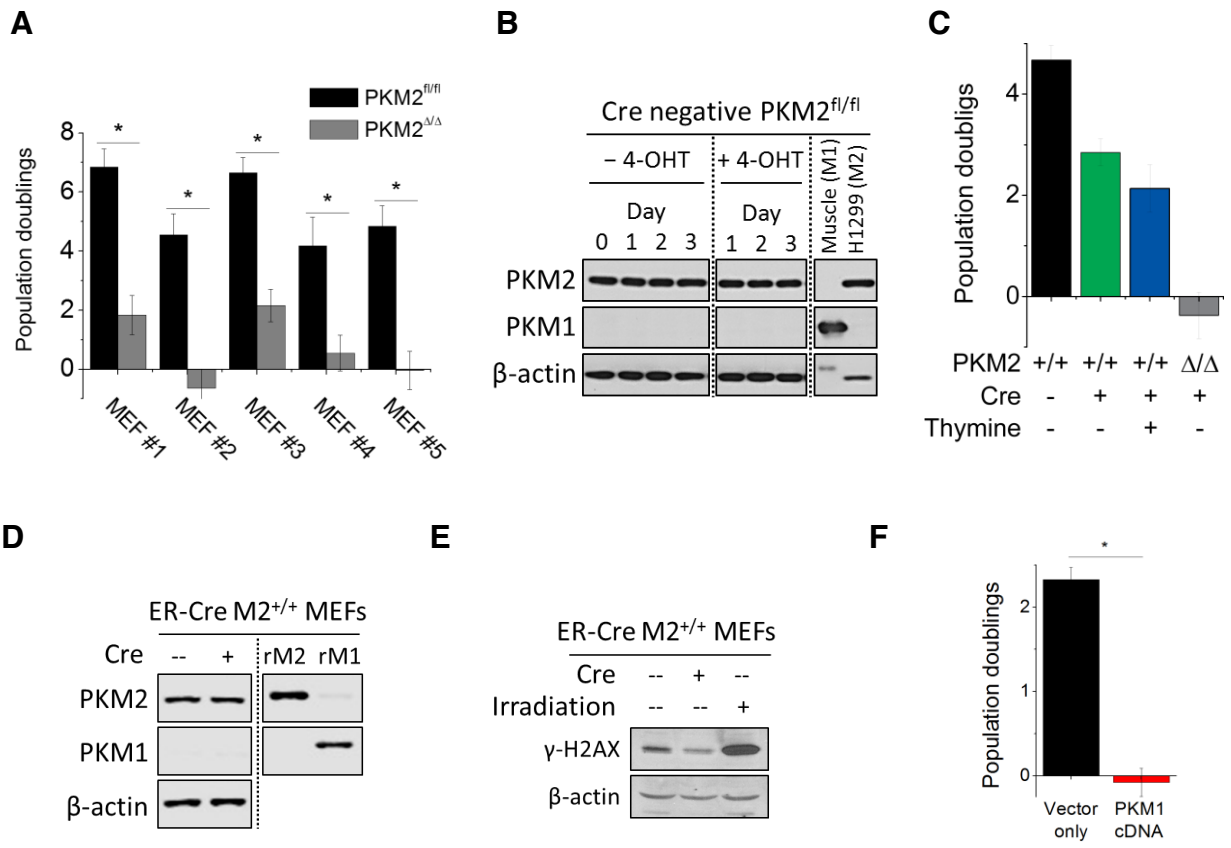

Figure S1. Proliferation arrest in MEFs isolated from different mice, related to Figure 1.

(A) Population doublings over 10 days of *PKM2*$^{\Delta/\Delta}$ MEFs generated from five different *PKM2*$^{fl/fl}$ *Cre-ER* mice following vehicle or 4-hydroxytamoxifen (4-OHT) treatment of *PKM2*$^{fl/fl}$ MEFs. Data are displayed as means ± SEM, n=3 (*p < 0.05).

(B) Western blot analysis of Cre negative *PKM2*$^{fl/fl}$ MEFs following vehicle or 4-OHT treatment. Western blots of lysate from mouse muscle or H1299 cancer cells are included as controls for PKM1 and PKM2 expression, respectively.

(C) Population doublings over 10 days of MEFs generated from *PKM2*$^{+/+}$ *Cre-ER* mice following vehicle, 4-hydroxytamoxifen (4-OHT), or 4-OHT plus 250 μM thymine supplementation. *PKM2*$^{\Delta/\Delta}$ MEFs generated from *PKM2*$^{fl/fl}$ *Cre-ER* mice following 4-OHT treatment are also shown for comparison. Data are displayed as means ± SEM, n=3.

(D) Western blot analysis of MEFs generated from *PKM2*$^{+/+}$ *Cre-ER* mice. 4-OHT treatment does not affect pyruvate kinase isoform expression. Western blot analysis of 100 ng of recombinant PKM1 or PKM2 (rPKM1, rPKM2) are included as controls.

(E) Western blot analysis of MEFs generated from *PKM2*$^{+/+}$ *Cre-ER* mice with vehicle or 4-OHT treatment. Irradiated MEFs are included as controls.

(F) Population doublings over 10 days of wildtype MEFs with pLHCX vector only or with exogenous expression of PKM1 cDNA. Data are displayed as means ± SEM, n=3 (*p < 0.05).

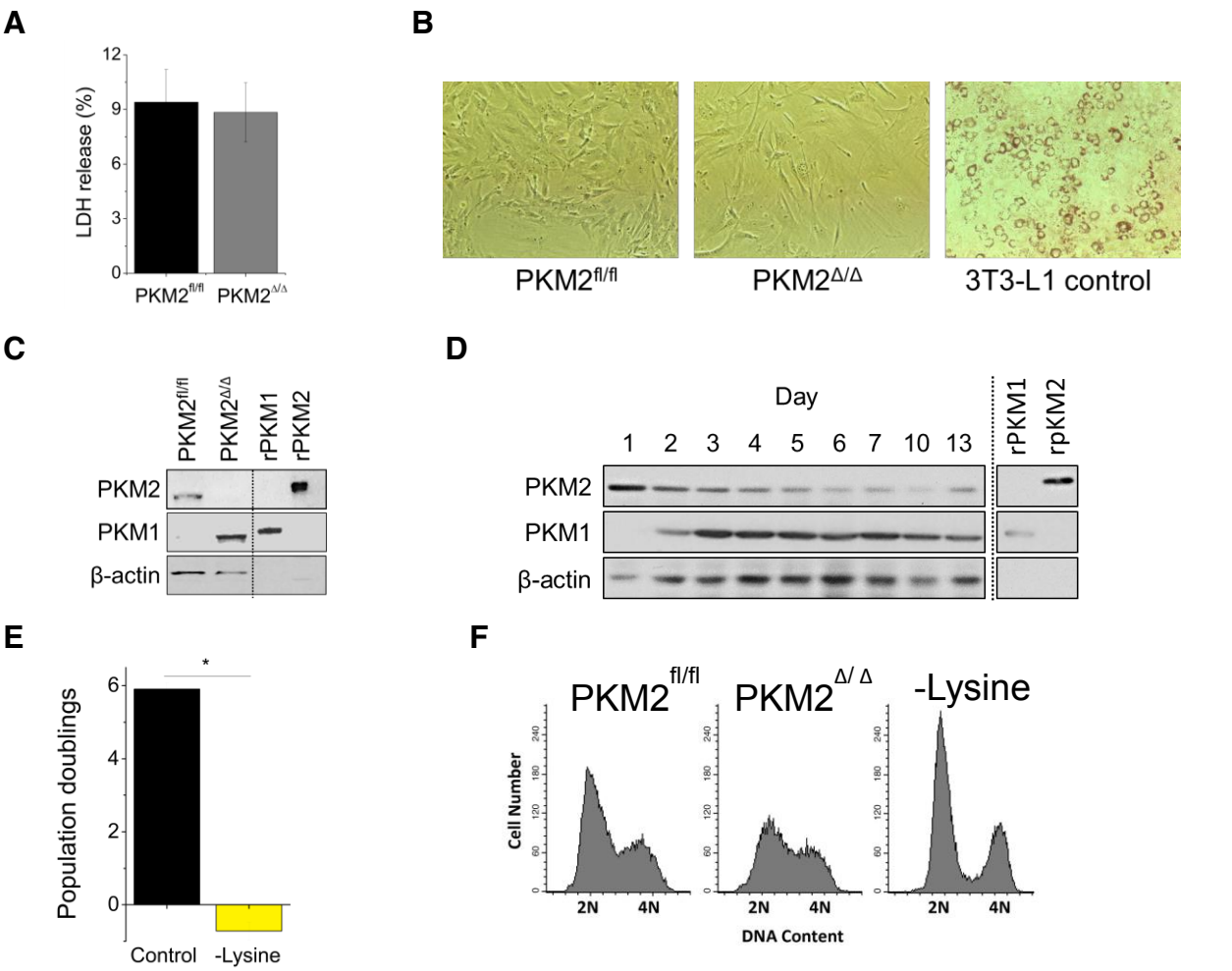

Figure S2. *PKM2*$^{\Delta/\Delta}$ cells undergo proliferation arrest without cell death or differentiation, and the arrest is different from cell cycle arrest triggered by nutrient deprivation, related to Figure 2.

(A) Quantification of cell death over a 24 h period by LDH release after treatment of *PKM2*$^{fl/fl}$ MEFs with vehicle (*PKM2*$^{fl/fl}$) or 4-OHT (*PKM2*$^{\Delta/\Delta}$). Data are displayed as means ± SEM, n=3.

(B) Oil Red O staining of *PKM2*$^{fl/fl}$ and *PKM2*$^{\Delta/\Delta}$ MEFs 6 days after treatment with vehicle or 4-OHT. The right pane shows a positive control of wildtype immortalized MEFs differentiated into adipocytes by expression of PPARγ.

(C) Western blot analysis of *PKM2*$^{fl/fl}$ and *PKM2*$^{\Delta/\Delta}$ myoblasts 9 days after treatment with vehicle or 4-OHT.

(D) Western blot analysis of primary myoblasts following incubation in low-serum media to induce differentiation into myotubes. Western blot analysis of 100 ng of recombinant PKM1 or PKM2 (rPKM1, rPKM2) are included as controls for both panels.

(E) Population doublings over 10 days of MEFs generated from wildtype mice in regular DMEM media or DMEM media without lysine. Data are displayed as means ± SEM, n=3 (*$p < 0.05$).

(F) DNA content was assessed using propidium iodide staining and flow cytometry in *PKM2*$^{fl/fl}$ MEFs, *PKM2*$^{\Delta/\Delta}$ MEFs, and MEFs cultured in media without lysine.

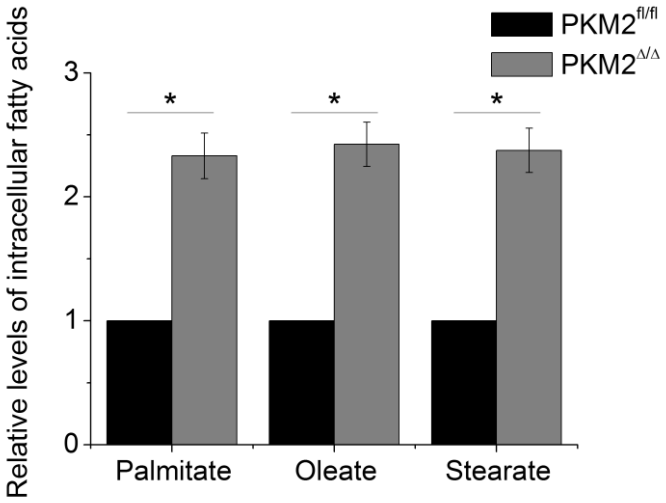

Figure S3. Levels of intracellular fatty acids, related to Figure 3. Fatty acids were extracted from *PKM2*$^{fl/fl}$ and *PKM2*$^{\Delta/\Delta}$ MEFs 7 days after treatment of *PKM2*$^{fl/fl}$ MEFs with vehicle or 4-OHT. All data are displayed as means ± SEM, n=3 (*p < 0.05).

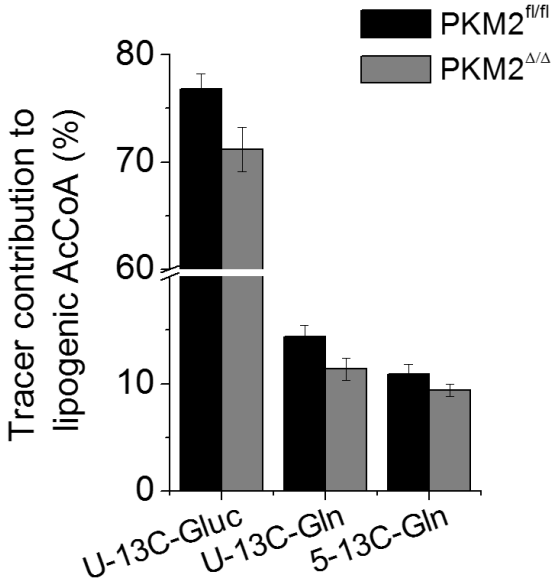

Figure S4. Less palmitate is synthesized from glucose and glutamine in *PKM2*$^{\Delta/\Delta}$ MEFs relative to *PKM2*$^{fl/fl}$ MEFs, related to Figure 4. The relative contribution of [U-^{13}C]glucose, [U-^{13}C]glutamine, and [5-^{13}C]glutamine to newly synthesized palmitate in *PKM2*$^{fl/fl}$ and *PKM2*$^{\Delta/\Delta}$ MEFs 7 days after *PKM2*$^{fl/fl}$ *Cre-ER* MEFs were treated with vehicle or 4-OHT was determined as described previously (Fendt et al., 2013; Metallo et al., 2012). Data are displayed as means ± SEM, n=3 (*p < 0.05).

A

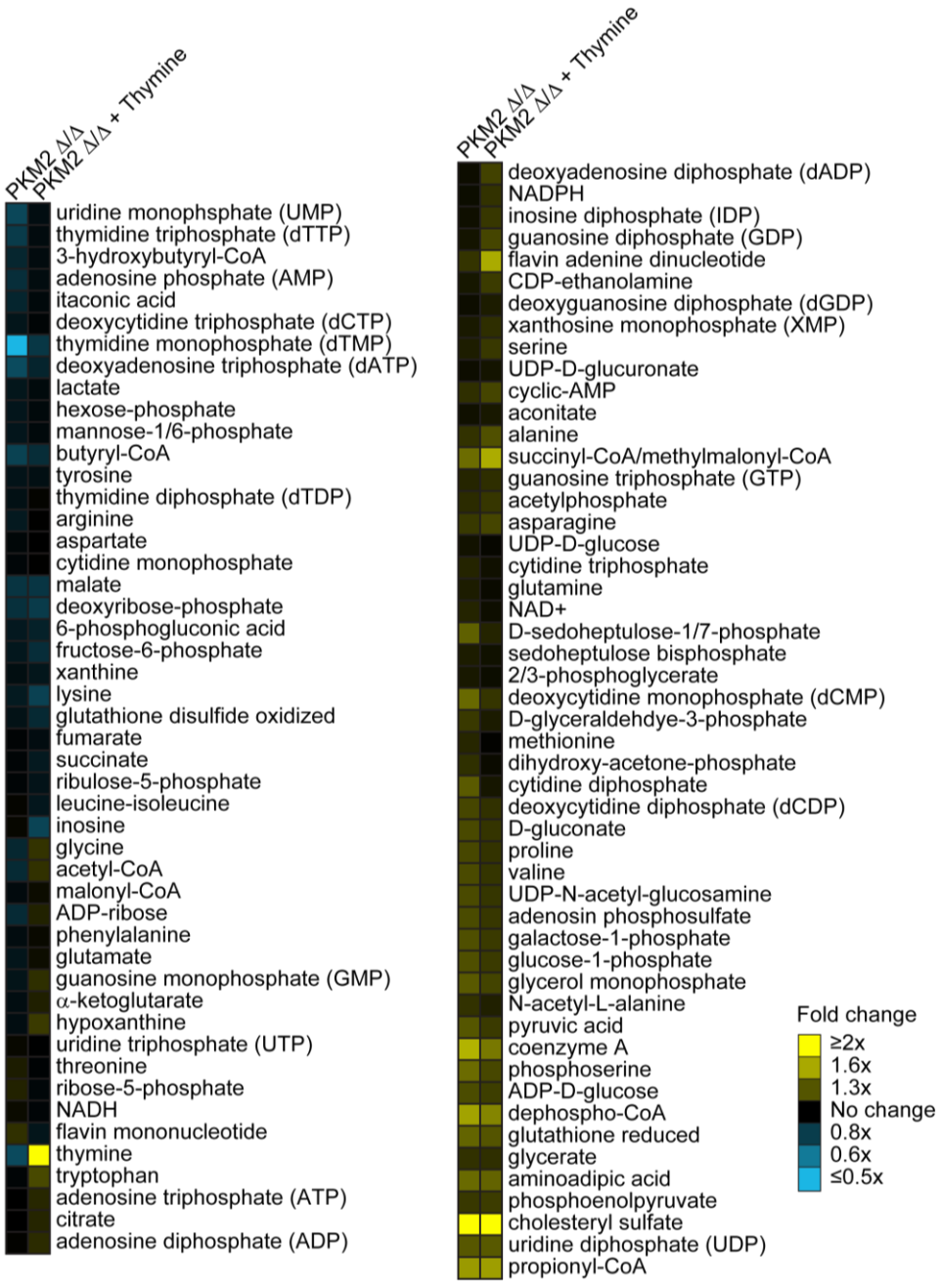
PKM2 Δ/Δ
PKM2 Δ/Δ + Thymine
uridine monophsphate (UMP)
thymidine triphosphate (dTTP)
3-hydroxybutyryl-CoA
adenosine phosphate (AMP)
itaconic acid
deoxycytidine triphosphate (dCTP)
thymidine monophosphate (dTMP)
deoxyadenosine triphosphate (dATP)
lactate
hexose-phosphate
mannose-1/6-phosphate
butyryl-CoA
tyrosine
thymidine diphosphate (dTDP)
arginine
aspartate
cytidine monophosphate
malate
deoxyribose-phosphate
6-phosphogluconic acid
fructose-6-phosphate
xanthine
lysine
glutathione disulfide oxidized
fumarate
succinate
ribulose-5-phosphate
leucine-isoleucine
inosine
glycine
acetyl-CoA
malonyl-CoA
ADP-ribose
phenylalanine
glutamate
guanosine monophosphate (GMP)
α-ketoglutarate
hypoxanthine
uridine triphosphate (UTP)
threonine
ribose-5-phosphate
NADH
flavin mononucleotide
thymine
tryptophan
adenosine triphosphate (ATP)
citrate
adenosine diphosphate (ADP)
PKM2 Δ/Δ
PKM2 Δ/Δ + Thymine
deoxyadenosine diphosphate (dADP)
NADPH
inosine diphosphate (IDP)
guanosine diphosphate (GDP)
flavin adenine dinucleotide
CDP-ethanolamine
deoxyguanosine diphosphate (dGDP)
xanthosine monophosphate (XMP)
serine
UDP-D-glucuronate
cyclic-AMP
aconitate
alanine
succinyl-CoA/methylmalonyl-CoA
guanosine triphosphate (GTP)
acetylphosphate
asparagine
UDP-D-glucose
cytidine triphosphate
glutamine
NAD+
D-sedoheptulose-1/7-phosphate
sedoheptulose bisphosphate
2/3-phosphoglycerate
deoxycytidine monophosphate (dCMP)
D-glyceraldehdye-3-phosphate
methionine
dihydroxy-acetone-phosphate
cytidine diphosphate
deoxycytidine diphosphate (dCDP)
D-gluconate
proline
valine
UDP-N-acetyl-glucosamine
adenosin phosphosulfate
galactose-1-phosphate
glucose-1-phosphate
glycerol monophosphate
N-acetyl-L-alanine
pyruvic acid
coenzyme A
phosphoserine
ADP-D-glucose
dephospho-CoA
glutathione reduced
glycerate
aminoadipic acid
phosphoenolpyruvate
cholesteryl sulfate
uridine diphosphate (UDP)
propionyl-CoA
Fold change
≥2x
1.6x
1.3x
No change
0.8x
0.6x
≤0.5x

B

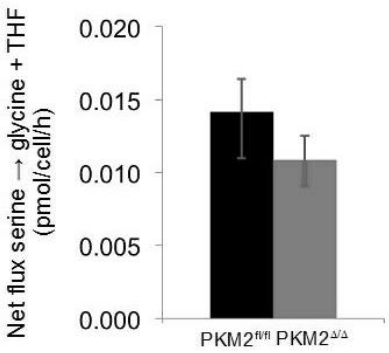
Net flux serine → glycine + THF
(pmol/cell/h)
0.020
0.015
0.010
0.005
0.000
PKM2fl/fl PKM2Δ/Δ

Figure S5. Pyruvate kinase isoform expression affects cellular metabolism, related to Figure 5.

(A) Profiles of intracellular metabolites in *PKM2*$^{\Delta/\Delta}$ MEFs without or with 250 μM thymine supplementation 7 days after treatment of *PKM2*$^{fl/fl}$ MEFs with vehicle or 4-OHT, as determined by GC-MS or LC-MS/MS. Relative levels are expressed as the log ratio of the normalized signal intensity in *PKM2*$^{\Delta/\Delta}$ MEFs to the normalized signal intensity in the *PKM2*$^{fl/fl}$ MEFs. Signal intensity was also normalized by total protein content to account for the difference in size between *PKM2*$^{fl/fl}$ and *PKM2*$^{\Delta/\Delta}$ MEFs (n=3).

(B) Net serine to glycine and THF flux in PKM2$^{fl/fl}$ and PKM2$^{\Delta/\Delta}$ MEFs. Fluxes were modeled based on ^{13}C glucose labeling in serine and glycine and the serine and glycine uptake rates. Differences between PKM2$^{fl/fl}$ and PKM2$^{\Delta/\Delta}$ MEFs are not significant based on 95% confidence intervals.

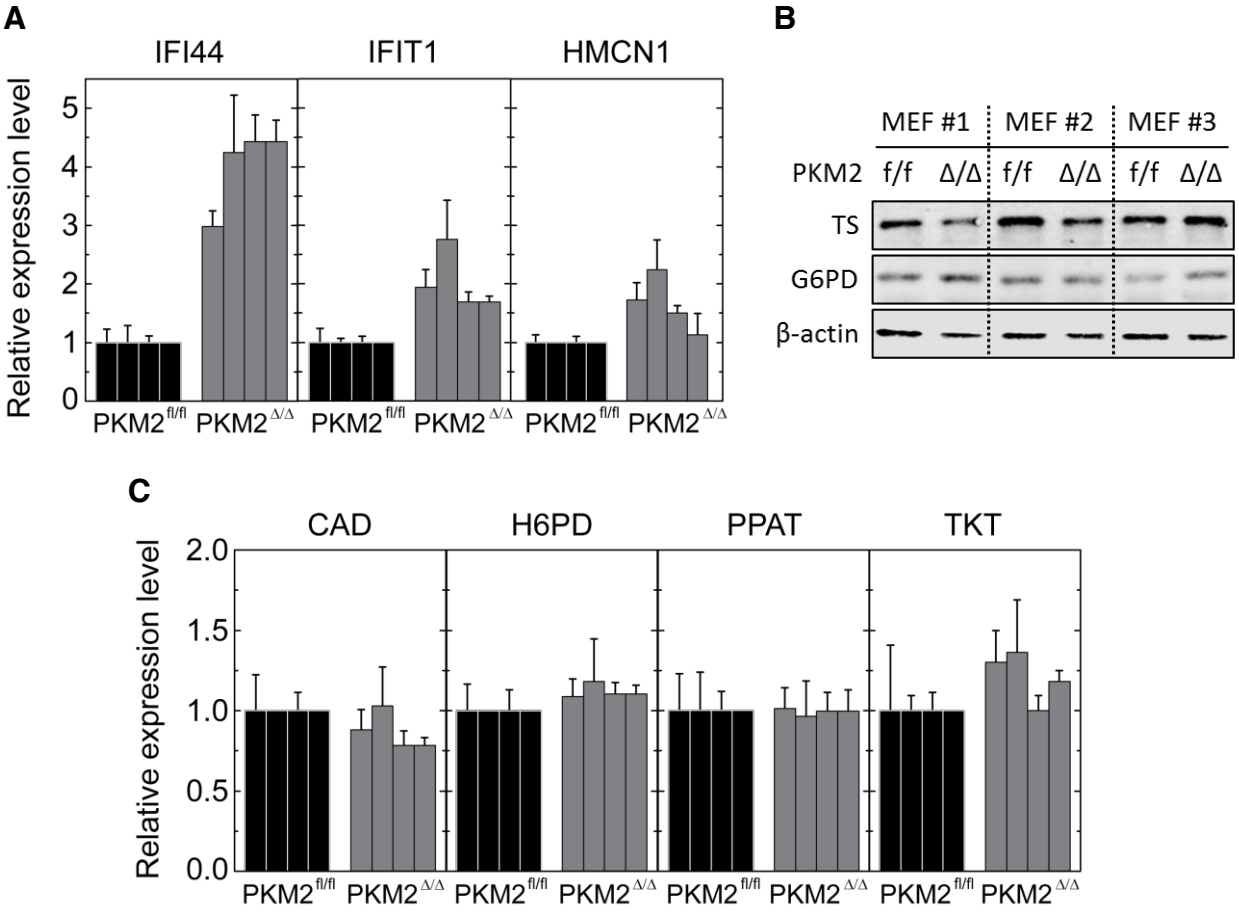

Figure S6. Expression analysis of select genes and proteins, related to Figure 6.
(A) Quantitative RT-PCR results for genes identified to have the largest difference in gene expression from analysis using Affymetrix GeneChip Mouse Gene 1.0 ST array: Interferon Induced Protein 44 (IFI44); Interferon-Induced Protein With Tetratricopeptide Repeats 1 (IFIT1); Hemicentin 1 (HMCN1). RNA was isolated from *PKM2*$^{fl/fl}$ and *PKM2*$^{\Delta/\Delta}$ MEFs derived from four independent *PKM2*$^{fl/fl}$ *Cre-ER* embryos 7 days following vehicle or 4-OHT addition. Data are displayed as means ± SEM, n=3.
(B) Western blot analysis of protein lysates from *PKM2*$^{fl/fl}$ and *PKM2*$^{\Delta/\Delta}$ MEFs derived from three independent *PKM2*$^{fl/fl}$ *Cre-ER* embryos for enzymes involved in nucleotide biosynthesis: thymidylate synthase (TS); Glucose-6-phosphate dehydrogenase (G6PD). *PKM2*$^{fl/fl}$ *Cre-ER* MEFs were treated with 4-OHT (*PKM2*$^{\Delta/\Delta}$) or vehicle (*PKM2*$^{fl/fl}$) for 7 days before collecting protein lysates.
(C) Quantitative RT-PCR results for genes involved in nucleotide biosynthesis: Carbamoyl-Phosphate Synthetase 2, Aspartate Transcarbamylase, and Dihydroorotase (CAD); Glucose-6-Phosphate Dehydrogenase (H6PD); Phosphoribosyl Pyrophosphate Amidotransferase (PPAT); Transketolase (TKT). RNA was isolated from *PKM2*$^{fl/fl}$ and *PKM2*$^{\Delta/\Delta}$ MEFs derived from four independent *PKM2*$^{fl/fl}$ *Cre-ER* embryos 7 days following vehicle or 4-OHT addition. Data are displayed as means ± SEM, n=3.

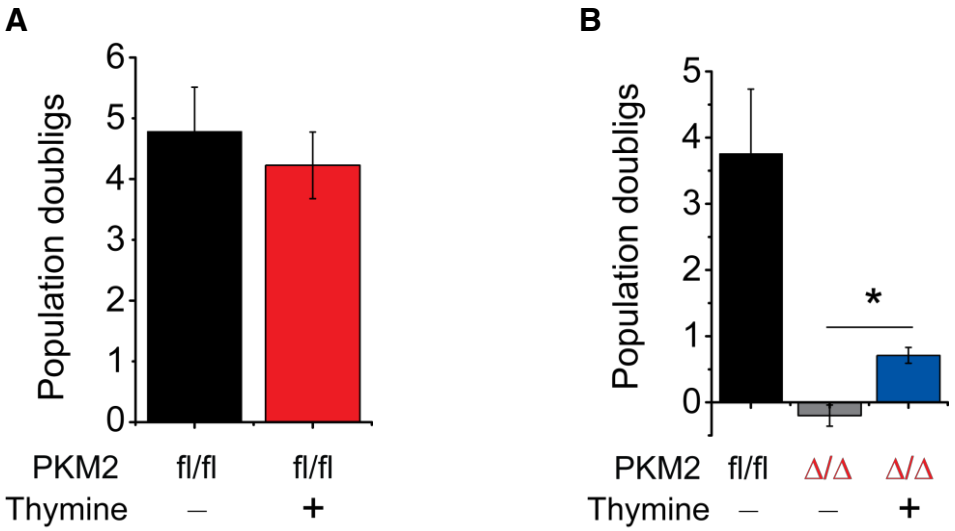

Figure S7. Exogenous thymine supplementation affects *PKM2*$^{\Delta/\Delta}$, but not *PKM2*$^{fl/fl}$, MEF proliferation, related to Figure 7.

(A) Population doublings over 10 days of *PKM2*$^{fl/fl}$ MEFs were measured with or without thymine supplemented in the media at a concentration of 250 μM. Data are displayed as means ± SEM, n=3.

(B) Population doublings over 10 days of *PKM2*$^{fl/fl}$ and *PKM2*$^{\Delta/\Delta}$ MEFs. 250 μM thymine was added on day 5 after addition of 4-OHT when *PKM2*$^{\Delta/\Delta}$ MEFs had stopped proliferating. All proliferation of *PKM2*$^{\Delta/\Delta}$ MEFs occurred between day 5 and 10 after thymine addition. Data are displayed as means ± SEM, n=3. *The difference in population doubling of *PKM2*$^{\Delta/\Delta}$ MEFs with and without thymine supplementation is statistically significant ($p < 0.05$).

Table S1 included as Excel spreadsheet. Mass isotopomer distributions (MIDs) of measured intracellular metabolites, related to Figure 5. MIDs of all metabolites were measured by GCMS, except for MIDs of UMP and hexose phosphate, which were measured by LC-MS/MS. Numbers shown are average fraction of each isotopomer ± SEM, n=3. MIDs have been corrected for natural isotope abundance.

Table S2 included as Excel spreadsheet. Mass isotopomer distributions (MIDs) of measured intracellular metabolites over time, related to Figure 5. MIDs of all metabolites were measured by LC-MS/MS. Numbers shown are average fraction of each isotopomer ± SEM, n=3. MIDs have been corrected for natural isotope abundance.

SUPPLEMENTAL EXPERIMENTAL PROCEDURES

All mouse studies were performed in accordance with institutional guidelines and approved by the MIT committee on animal care.

Isolation and culture of primary mouse embryonic fibroblasts

Primary mouse embryonic fibroblasts (MEFs) were isolated and cultured using an adaption of previously published methods (Springer et al., 2001). Embryos were isolated from the uterus of pregnant mice staged E11.5 – E14.5 of gestation and decapitated in PBS. Each embryo was processed separately due to heterogeneity in genetic background. After removing blood and organ tissue from each embryo, each was homogenized, resuspended in 2 ml of 0.25% warm trypsin, and incubated at 37°C for 30 min. To break up genomic DNA, 5 ml of HBSS with $CaCl_2$ and $MgCl_2$ was first added to each tube, and treated with 5 µl of $5\mu g \cdot \mu l^{-1}$ DNase. The mixture was incubated at 37°C for 5 - 15 min. The supernatant was collected and transferred to a fresh tube on ice. Additional 2 ml of 0.25% trypsin was added to the remaining tissue pieces and incubated at 37°C for 30 min and again treated with HBSS and DNase. The supernatant was collected and added to the previous tube of cells on ice. Cells were pelleted, resuspended in MEF medium (Dulbecco's Modified Eagle's Medium with 10% heat inactivated FBS, 1% streptomycin/penicillin, 1 mM glutamine, and 0.1 mM 2-mercaptoethanol) and plated at a density of 5×10^6 cells per 10 cm plate. Cells were split before reaching confluence and replated at 750,000 cells per 10 cm plate, or frozen in 3×10^6 cell aliquots. 1 µM 4-hydroxytamoxifen dissolved in ethanol was used to induce recombination of *PKM2*^{fl} alleles. Cells starved of lysine were incubated in lysine-free DMEM and doubling time analyzed over 10 days.

Isolation and culture of primary myoblasts

Primary myoblasts were isolated and cultured using an adaptation of previously published methods (Rando and Blau, 1994; Springer et al., 2001). Muscle was isolated from 2 – 2.5 week old mice and mechanically disaggregated, followed by enzymatic disaggregation with Collagenase P (10 $mg \cdot ml^{-1}$ in PBS; Roche) at 37°C for 45 min with trituration every 15 min. The slurry was passed through a 70µm filter, and additional PBS was added to dilute out collagenase. Cells were pelleted by centrifugation and pre-plated on a non-treated tissue culture plate for 4 h to remove fibroblasts. Unattached myoblasts were re-plated in 0.1% gelatin coated plates in F-10-based primary myoblast growth medium (Ham's F10 medium with 10% Cosmic calf serum (Hyclone), 1% streptomycin/penicillin, 1 mM glutamine, and 2.5 $ng \cdot ml^{-1}$ basic fibroblast growth factor (PeproTech)). Medium was changed every 2 days, and cells were split before reaching confluence, at no more than 1:5 dilution. Myoblasts are capable of differentiation into myotubes when cultured under conditions that promote differentiation (Springer et al., 2001). For differentiation into myotubes, cells were cultured in low-serum medium: Dulbecco's Modified Eagle's Medium with 5% horse serum, 1% streptomycin/penicillin, and 1 mM glutamine. Medium was changed daily. To prepare gelatin coated plates, 2% gelatin stock (Sigma-Aldrich) was warmed up to 37°C and diluted to a concentration of 0.1% in PBS. Approximately 7 ml of the diluted 0.1% gelatin solution in PBS was added to each 10 cm plate and incubated at 37°C for at

least 1 h. The gelatin solution was aspirated, and plates were rinsed with fresh PBS before use.

Cell lysis and immunoblotting

Cell lysis and Western blot analysis were carried out according to standard protocols. The following dilutions of primary commercial antibodies were used as probes: 1:20000 dilution of anti-PKM1 (Sigma SAB4200094); 1:10000 dilution of anti-PKM2 (Cell Signaling 4053S); 1:500 dilution of anti-actin (Abcam ab8226); 1:1000 dilution of anti-γ-H2AX (EMD Millipore 05-636); 1:1000 dilution of anti-TS (Cell Signaling 9045); and 1:1000 dilution of anti-G6PD (Cell Signaling 12263). Primary antibodies were diluted in 5% BSA containing 0.1% azide and incubated overnight at 4°C. Secondary antibodies were diluted in 5% BSA at a dilution of 1:10000.

Cell cycle analysis

Cells were centrifuged at 1000g for 5 minutes and washed twice in PBS. The cell pellet was resuspended in 500 µl of ice-cold PBS. To fix the cells, 5 ml of ice cold ethanol was added to the cell suspension. Cells were fixed at 4°C at least overnight. Just before analysis, fixed cells were centrifuged at 1000g and washed twice in PBS with 1% BSA. Cells were treated with RNase and resuspended in the wash buffer with propidium iodide added to a final concentration of 50 $\mu g \cdot ml^{-1}$. Cells were analyzed for propidium iodide (JM-1056, from MBL Int'l.) content on a Becton Dickinson FACScan flow cytometer; a laser with wavelength 488 nm was used for excitation and emission measured at 585 nm. To assay for new DNA synthesis, the Click-iT EdU Alexa Fluor 488 kit was used (Invitrogen C35002). 10 µM of EdU was used for a 3 hour incubation. Cells were imaged on a Nikon Eclipse TE2000-U microscope with a 4 second exposure time and analyzed using the ImageJ software. Cells were dual stained for DNA content and new DNA synthesis with the Click-iT EdU Alexa Fluor 488 Kit and FxCycle Violet Stain (Life Technologies F-10347), respectively, and cells were analyzed on the BD FACSCanto II using FACS Diva software. Viability was assessed by propidium iodide dye exclusion. Trypsinized cells were resuspended in PBS + 1% BSA with 2 µg/mL propidium iodide and analyzed using a BD FACScan.

Senescence-associated β-galactosidase staining and LDH assay for cell death

Cells were plated at a density of 125,000 cells per well of 6-well plates on day 0 with vehicle or 4-OHT treatment. At indicated days following seeding, senescence-associated β-galactosidase activity was detected using previously described methods (Debacq-Chainiaux et al., 2009). LDH was measured using the Roche Cytotoxicity Detection Kit (Roche 11644793001).

Metabolite extraction and analysis

For metabolite analysis using gas chromatography/mass spectrometry, cells were cultured for ~72 h in 6-well plates in glucose- and glutamine-free DMEM (Sigma D5030) containing 10% dialyzed FBS, 1% streptomycin/penicillin, 4 mM glutamine or 25 mM glucose, and the appropriate tracer, [U-$^{13}C_6$]glucose, [U-$^{13}C_5$]glutamine, or [5-^{13}C]glutamine (all from Cambridge Isotopes Laboratories, Inc). After incubation, media was aspirated, and each well was rinsed with 1 ml ice-cold saline. Saline was aspirated, and cells were quenched with 500 µl of -20°C HPLC-grade methanol. 300 µl

of ice-water was added, and cells were scraped with a 1000 µl pipette tip and collected in 1.5 ml Eppendorf tubes. 500 µl of -20°C chloroform was added to each tube and vortexed for 10 min at 4°C. Extracts were centrifuged at 14,000*g* for 5 min at 4°C. The upper aqueous phase was collected in a separate tube evaporated under nitrogen for polar metabolite analysis. The lower layer was collected in a separate tube and evaporated under nitrogen for nonpolar metabolite analysis. Metabolites were derivatized and analyzed using gas chromatography/mass spectrometry as previously described (Fendt et al., 2013; Metallo et al., 2012). The rate of fatty acid synthesis was calculated as previously described (Fendt et al., 2013).

For metabolite analysis using liquid chromatography tandem mass spectrometry (LC-MS/MS), cells were cultured for ~24 h in 10 cm plates. After incubation, media was aspirated, and each plate was rinsed with 10 ml ice-cold saline. Saline was aspirated, and cells were quenched with 2.89 ml of -20°C HPLC-grade methanol. 1.74 ml of ice-water was added, and cells were scraped with a cell lifter and collected in 15 ml conical tubes. 2.89 ml of -20°C chloroform was added to each tube and vortexed for 10 min at 4°C. Extracts were centrifuged at 4,000g for 15 min at 4°C. The upper aqueous phase was collected in a separate tube evaporated under nitrogen for polar metabolite analysis. LC-MS/MS analysis was done using a variation of the method described previously (Munger et al., 2008). A Paradigm MS4 HPLC (Michrom Bioresources, Auburn, CA), and a Synergi Hydro column (4 µm particle size, 80 Å, 150 mm × 2 mm, from Phenomenex) were used for separation of metabolites by polarity. Prior to column separation, samples were loaded onto a trapping column (C18, 4 mm × 2 mm, from Phenomenex) and washed for 30 seconds with HPLC grade water containing 10 mM tributylamine and 15 mM acetic acid for rapid desalting. HPLC separation was coupled with negative-mode electrospray ionization (ESI) to a TSQ Vantage Triple Stage Quadrupole Mass Spectrometer (Thermo Scientific) operating in multiple reaction monitoring (MRM) mode. The LC parameters were as follows: autosampler temperature, 10 ºC; injection volume, 10 µl; column temperature, room temperature; and flow rate, 200 $\mu l \cdot min^{-1}$. The LC solvents were Solvent A: 10 mM tributylamine and 15 mM acetic acid in 97:3 water:methanol (pH 4.95); and Solvent B: methanol. Elution from the column was performed over 50 min with the following gradient: t = 0, 0% B; t = 5, 0% B; t = 10, 20% B; t = 20, 20% B; t = 35, 65% B; t = 38, 95% B; t = 42, 95% B, t = 43, 0% B; t = 50, 0% B. ESI spray voltage was 3,000 V. Nitrogen was used as the sheath gas at 30 psi and as the auxiliary gas at 10 psi, and argon as the collision gas at 1.5 mTorr, with the capillary temperature at 325 ºC. Scan time for each MRM transition was 0.1 s with a scan width of 1 m/z. The LC runs were divided into time segments, with the MRM scans within each time segment containing compounds eluting during that time interval. For compounds eluting near boundaries between time segments, the MRM scan corresponding to the compound was conducted in both time segments. Instrument control, chromatographic control, and data acquisition were performed by the Xcalibar software (Thermo Scientific).

Data analysis was performed using MAVEN (Clasquin et al., 2012; Melamud et al., 2010). Pool sizes were first normalized by total protein of extracted cells. The protein content of extracted cells was determined from the dried protein fraction from each extraction, which was incubated overnight in 2 ml of 0.2 M KOH, and quantified by

Bradford assay. Isotope labeling data was corrected for the natural abundance of different isotopes using IsoCor (Millard et al., 2012).

CO_2 production from glucose

To assay $^{14}CO_2$ production from ^{14}C-labeled glucose, cells were incubated in 5 $\mu Ci \cdot ml^{-1}$ uniformly labeled (American Radiolabeled Chemicals #0122A) glucose for 24 hours. Carbon dioxide was trapped on a tight-fitting piece of Whatman paper that had been saturated with a solution of $Ba(OH)_2$; the resulting reaction between emitted CO_2 and $Ba(OH)_2$ resulted in a barium bicarbonate precipitate that was retained on the paper. The paper overlying each well was counted in 10 ml of scintillation fluid using a Beckman Coulter LS6500 Scintillation Counter. Total $^{14}CO_2$ emission was calculated by subtracting background radioactivity from the radioactivity on the filter paper.

Exogenous PKM1 expression

Standard retroviral infection protocol was used to introduce PKM1 expression constructs or delivery of an empty vector control (pLHCX). Briefly, target cells were incubated in virus-containing media produced from an HEK-293T packaging line for 24 hours. Media was changed and the cells were allowed to recover in standard media for 24 hours before they were incubated with hygromycin (100 µg/mL) for 5 days with daily media changes. During antibiotic selection and proliferation analysis, cells were passaged to a confluence of 750,000 cells per 10 cm plate every 3 days.

Gene expression analysis

Primary MEFs derived from two independent embryos were treated with vehicle or 4-OHT treated as previously described. The growth medium was removed 7 days following vehicle or 4-OHT addition, and cells were lysed on the dish using TRIzol Reagent (Life Technologies); RNA was isolated according to the manufacturer's protocol and RNA pellets were resuspended in DEPC-treated water. Microarray analysis was performed by the MIT BioMicro Center. Briefly, RNA quantity and quality were determined using an Agilent 2100 BioAnalyzer prior to sample preparation and hybridization to an Affymetrix GeneChip Mouse Gene 1.0 ST array. The intensity (.CEL) files were RMA normalized using Affymetrix Expression Console. Unsupervised hierarchical clustering was performed with Cluster 3.0. Genes were filtered based on standard deviation. Genes and arrays were centered at the mean prior to clustering genes and arrays using complete linkage methods and the correlation (uncentered) similarity metric. Probe identifiers were converted to gene names using DAVID (Huang et al., 2008, 2009). Clustering results were visualized with JavaTreeView. Figures were converted to a full-spectrum color scale using Matlab. Fold change analysis was conducted using Significance Analysis of Microarrays tool (Tusher et al., 2001) featured in the MuliExperiment Viewer within the TM4 Microarray Software Suite (Saeed et al., 2003). Microarray data are available on Gene Expression Omnibus (GEO), accession number GSE60499.

Retroviral Infection

A standard retroviral infection protocol was used to introduce expression constructs for PKM1 or an empty vector control (pLHCX). Briefly, HEK-293T cells were incubated for

36 hours in media containing 3 μg of the EcoPak packaging DNA and 3 μg of the vector of interest. Target cells were then incubated in the virus-containing media for 24 hours. Media was changed and the cells were allowed to recover in standard media for 24 hours before they were incubated with hygromycin (100 μg/mL) for 5 days with daily media changes. During antibiotic selection and proliferation analysis, cells were passaged to a confluence of 750,000 cells per 10 cm plate every 3 days.

RNA

RNA was isolated from *PKM2*$^{fl/fl}$ and *PKM2*$^{\Delta/\Delta}$ MEFs derived from *PKM2*$^{fl/fl}$ *Cre-ER* embryos 7 days following vehicle or 4-OHT addition using the Qiagen RNeasy Mini Kit (Qiagen 74104). Quantitative RT-PCR was performed using the QuantiTect SYBR Green RT-PCR kit (Qiagen 204243). Primer sequences for RT-PCR were the following:

Actin-F: CATCATGCGTCTGGACCTG
Actin-R: CTCACGTTCAGCTGTGGTCA

CAD-F: CGTGGAGACCATTGAACTGA
CAD-R: GCCTGAGCCTGTTCAAGAGA

CPT1-F: TCAAGAATGGCATCATCACTG
CPT1-R: GGAGGGGTCCACTTTGGTAT

H6PD-F: GCAGGTGTCCTTGTCCACAT
H6PD-R: ACGCCCGATTCTTAAACACA

HMCN1-F: TGTGAATGAAGATGCTGGTGA
HMCN1-R: TTCCACTGGCTCAAGAGTGA

IFI44-F: AACATGGCATTCTGCATTTG
IFI44-R: AATGCCTCCAGCTTGGACTT

IFIT1-F: ATGGGAGAGAATGCTGATGG
IFIT1-R: GAGATTCTCACTTCCAAATCAGG

PPAT-F: GAAGACCAAATGGTTTATACAGTAAGG
PPAT-R: CAGGCGTAGCAGACTCTGGA
TKT-F: TCACAGGGATTGAAGACAAGG
TKT-R: GGCCAGGATCTTCTTTTTGC.

Statistical analyses

Data are presented as means ± standard error of the mean (SEM). All *P* values were obtained using an unpaired two-tailed *t*-test, and statistical significance was determined at a value of 0.05.

13C-Metabolic flux analysis model included as Excel file.

Intracellular fluxes where modeled with the MatLab based software Metran (Antoniewicz et al., 2007; Young et al., 2008).

The flux model contains the following assumptions:

- Fluxes were modeled based on intracellular labeling of lactate, alanine, citrate, a-ketoglutarate, fumarate, malate, aspartate, glutamate, glutamine
- The system is in steady state. Unpublished data confirm that there is no significant difference in the labeling of polar metabolites after 24h or 72h
- All CO2 in the system is unlabeled
- Fumarate and succinate have no orientation, because they are symmetrical
- Any metabolite that is modeled in two different compartments is in equilibrium
- Entry of unlabeled pyruvate and AcCoA precursors is possible. Which is possible due to fatty acid oxidation or entry of amino acids from the media
- Flux to fatty acids is not constrained
- 3PG to serine flux was estimated with a specific serine/glycine flux model
- Biomass fluxes were based on Metallo et al 2009. The biomass fluxes were scaled for the total protein content of PKM1 and PKM2 cells and the measured growth rates
- Flux magnitude to NTPs was based on Metallo et al 2009 and scaled by EdU incooperation into DNA
- Pentose phosphate pathway flux was modeled as lower bound based on the flux to NTPs
- Glutamine to glutamate flux was calculated based on dynamic labeling data (Yuan et al., 2008).

Specific assumptions for serine/glycine model:

- Fluxes were modeled based on serine and glycine labeling
- Metran does not allow constraining net fluxes, therefore a forward flux for serine/glycine entry into the cell was modeled, while the reverse flux was modeled as serine/glycine sink. The difference of the forward and revers flux is the net flux, which was measured as serine/glycine uptake rate.

References

Antoniewicz, M.R., Kelleher, J.K., and Stephanopoulos, G. (2007). Elementary metabolite units (EMU): a novel framework for modeling isotopic distributions. Metabolic engineering *9*, 68-86.

Clasquin, M.F., Melamud, E., and Rabinowitz, J.D. (2012). LC-MS Data Processing with MAVEN: A Metabolomic Analysis and Visualization Engine. In Current Protocols in Bioinformatics (John Wiley & Sons, Inc.).

Debacq-Chainiaux, F., Erusalimsky, J.D., Campisi, J., and Toussaint, O. (2009). Protocols to detect senescence-associated beta-galactosidase (SA-[beta]gal) activity, a biomarker of senescent cells in culture and in vivo. Nat. Protocols *4*, 1798-1806.

Fendt, S.-M., Bell, E.L., Keibler, M.A., Olenchock, B.A., Mayers, J.R., Wasylenko, T.M., Vokes, N.I., Guarente, L., Heiden, M.G.V., and Stephanopoulos, G. (2013). Reductive glutamine metabolism is a function of the α-ketoglutarate to citrate ratio in cells. Nat Commun *4*.

Huang, D.W., Sherman, B.T., and Lempicki, R.A. (2008). Systematic and integrative analysis of large gene lists using DAVID bioinformatics resources. Nat. Protocols *4*, 44-57.

Huang, D.W., Sherman, B.T., and Lempicki, R.A. (2009). Bioinformatics enrichment tools: paths toward the comprehensive functional analysis of large gene lists. Nucleic Acids Research *37*, 1-13.

Melamud, E., Vastag, L., and Rabinowitz, J.D. (2010). Metabolomic Analysis and Visualization Engine for LC−MS Data. Analytical Chemistry *82*, 9818-9826.

Metallo, C.M., Gameiro, P.A., Bell, E.L., Mattaini, K.R., Yang, J., Hiller, K., Jewell, C.M., Johnson, Z.R., Irvine, D.J., Guarente, L.*, et al.* (2012). Reductive glutamine metabolism by IDH1 mediates lipogenesis under hypoxia. Nature *481*, 380-384.

Millard, P., Letisse, F., Sokol, S., and Portais, J.-C. (2012). IsoCor: correcting MS data in isotope labeling experiments. Bioinformatics *28*, 1294-1296.

Munger, J., Bennett, B.D., Parikh, A., Feng, X.J., McArdle, J., Rabitz, H.A., Shenk, T., and Rabinowitz, J.D. (2008). Systems-level metabolic flux profiling identifies fatty acid synthesis as a target for antiviral therapy. Nat Biotechnol *26*, 1179-1186.

Rando, T.A., and Blau, H.M. (1994). Primary mouse myoblast purification, characterization, and transplantation for cell-mediated gene therapy. The Journal of Cell Biology *125*, 1275-1287.

Saeed, A., Sharov, V., White, J., Li, J., Liang, W., Bhagabati, N., Braisted, J., Klapa, M., Currier, T., and Thiagarajan, M. (2003). TM4: a free, open-source system for microarray data management and analysis. Biotechniques *34*, 374.

Springer, M.L., Rando, T.A., and Blau, H.M. (2001). Gene Delivery to Muscle. In Current Protocols in Human Genetics (John Wiley & Sons, Inc.).

Tusher, V.G., Tibshirani, R., and Chu, G. (2001). Significance analysis of microarrays applied to the ionizing radiation response. Proceedings of the National Academy of Sciences *98*, 5116-5121.

Young, J.D., Walther, J.L., Antoniewicz, M.R., Yoo, H., and Stephanopoulos, G. (2008). An elementary metabolite unit (EMU) based method of isotopically nonstationary flux analysis. Biotechnol Bioeng *99*, 686-699.

Yuan, J., Bennett, B.D., and Rabinowitz, J.D. (2008). Kinetic flux profiling for quantitation of cellular metabolic fluxes. Nat Protoc *3*, 1328-1340.